AD-A121 491 THERMAL DIFFUSION IN CARBON/CARBON COMPOSITES(U) PURDUE 1/1
UNIV LAFAYETTE IND THERMOPHYSICAL PROPERTIES RESEARCH
CENTER R E TAYLOR ET AL. JUN 82 TPRL-256
UNCLASSIFIED AFOSR-TR-82-0959 F49620-81-K-0011 F/G 11/4 NL

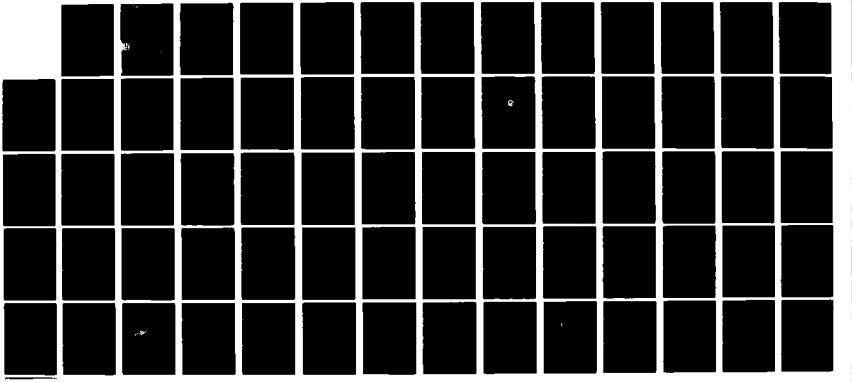

END

FILMED
1
DTIC

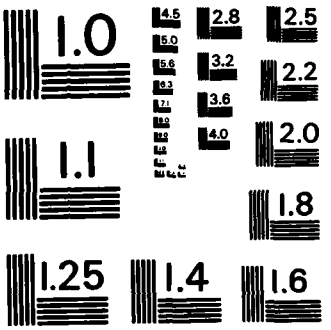

MICROCOPY RESOLUTION TEST CHART
NATIONAL BUREAU OF STANDARDS-1963-A

TPRL

THERMOPHYSICAL PROPERTIES RESEARCH LABORATORY

AFOSR-TR- 82-0959

TPRL 256

THERMAL DIFFUSION IN CARBON/ CARBON COMPOSITES

Special Report for AFOSR Grant F 49620-81-K-0011

by

R.E. Taylor, J. Jortner and H. Groot

June, 1982

School of Mechanical Engineering

Purdue University, West Lafayette, Indiana

SECURITY CLASSIFICATION OF THIS PAGE (When Data Entered)

REPORT DOCUMENTATION PAGE

READ INSTRUCTIONS BEFORE COMPLETING FORM

1. REPORT NUMBER: AFOSR-TR- 82-0959	2. GOVT ACCESSION NO.: A121 491
3. RECIPIENT'S CATALOG NUMBER:	
4. TITLE (and Subtitle): Thermal Diffusion in Carbon/Carbon Composites	5. TYPE OF REPORT & PERIOD COVERED: 15 Feb. 1981 - 30 Jan. 1982
	6. PERFORMING ORG. REPORT NUMBER: TPRL 256
7. AUTHOR(s): R.E. Taylor, J. Jortner, and H. Groot	8. CONTRACT OR GRANT NUMBER(s): F 49620-81-K-0011
9. PERFORMING ORGANIZATION NAME AND ADDRESS: Thermophysical Properties Research Laboratory, Purdue University, West Lafayette, IN 47907	10. PROGRAM ELEMENT, PROJECT, TASK AREA & WORK UNIT NUMBERS: 61102 F, 2308/A1
11. CONTROLLING OFFICE NAME AND ADDRESS: Air Force Office of Scientific Research/NA, Bolling AFB, DC 20332	12. REPORT DATE: June, 1982
	13. NUMBER OF PAGES: 62
14. MONITORING AGENCY NAME & ADDRESS(if different from Controlling Office)	15. SECURITY CLASS. (of this report): Unclassified
	15a. DECLASSIFICATION/DOWNGRADING SCHEDULE

16. DISTRIBUTION STATEMENT (of this Report)

Approved for public release; distribution unlimited.

17. DISTRIBUTION STATEMENT (of the abstract entered in Block 20, if different from Report)

18. SUPPLEMENTARY NOTES

19. KEY WORDS (Continue on reverse side if necessary and identify by block number)

Carbon/Carbon Composites
Thermal Diffusivity
Thermal Conductivity
Transient Heat Flow
Temperature

20. ABSTRACT (Continue on reverse side if necessary and identify by block number)

Transient heat flow through carbon/carbon materials was studied. It was found that special steps must be taken to measure thermal diffusivity along the principal axes, especially at temperatures below about 500°C. However, the use of off-axis samples permited the unambigious determination of diffusivity values, not only in the off-axis directions, but also along the principal axes. Diffusivity results for the matrix and for the fiber bundles were also obtained directly and indirectly and the results were in reasonable agreement. It was shown that there is a surface layer in carbon/carbon materials in

DD FORM 1 JAN 73 1473

UNCLASSIFIED

SECURITY CLASSIFICATION OF THIS PAGE (When Data Entered)

20. ABSTRACT (continued)

which inter-constituent thermal gradients are significant and beyond which they are negligible. Carbon/carbon materials may be treated as homogeneous through regions which are much thicker than the heterogeneity dimension but in surface layers subjected to large heat fluxes, the heterogeneity must be considered.

TPRL 256

THERMAL DIFFUSION IN CARBON/CARBON COMPOSITES

Special Report for Air Force Office of Scientific Research

by

R.E. Taylor, J. Jortner and H. Groot

June, 1982

TABLE OF CONTENTS

		Page
I.	INTRODUCTION	1
II.	SAMPLE DESCRIPTION	4
III.	RESULTS	7
IV.	DISCUSSION	21
V.	REFERENCES	30
VI.	APPENDICES:	
	I. On the Use of Off-Axis Testing to Characterize the Thermal Diffusivities of Orthogonally Reinforced Carbon-Carbon Composites	31
	II. Analysis of Transient Temperature Response of a Carbon-Carbon Composite During Continuous Heating at One Surface	49

LIST OF TABLES

1.	Parameters Affecting Thermal Diffusivity Experiments	3
2.	Bulk Density Values	6
3.	Measured Unit Cell Dimensions (mm) and Calculated Yarn Bundle Fractions for On-Yarn Diffusivity Specimens from O.D. Region of Billet F-11	8
4.	Energy Materials Testing Laboratory Diffusivity Samples	9
5.	Thermal Diffusivity Results	10
6.	Thermal Diffusivity Results (Axial-2)	14
7.	Diffusivity Values as a Function of Position	16
8.	Diffusivity Values for a Fiber Bundle Experiment	17
9.	Diffusivity Results (EMTL)	18
10.	"Steady State" Thermal Diffusivity Results	22
11.	Calculated and Measured 45° Off-Axis Diffusivity Values	24

TABLE OF CONTENTS (continued)

LIST OF FIGURES

		Page
1.	Nomenclature for 3D Cylindrical Unit Cell and Sketch Showing Five Directions in which Diffusivity was measured	5
2.	Thermal Diffusivity Results	11
3.	Normalized Rear Face Temperature Rise for Axial-Circumferential Sample at 552°	13
4.	Location of Point-Source Temperature Sensing Probe (Axial-2 Sample)	15
5.	Comparison of EMTL and TPRL Diffusivity Results for Axial Samples	19
6.	Comparison of EMTL and TPRL Difusivity Results for Radial Samples	20
7.	"Steady-State" Diffusivity Values	23
8.	"Steady-State" Diffusivity Values Versus Fiber Fraction in Direction of Measurement	25
9.	Thermal Diffusivity of the Matrix as a Function of Temperature	26
10.	Thermal Diffusivity of the Fiber Bundles as a Function of Temperature	27

THERMAL DIFFUSION IN CARBON/CARBON COMPOSITES

I. INTRODUCTION

Thermal conductivity is the property used to relate heat fluxes to steady state temperature gradients. The application of standard thermal conductivity test methods to heterogeneous composites presents no particular difficulties, beyond the usual ones associated with this relatively difficult property determination.

The heat-balance equation for transient conditions may be written as

$$\nabla \cdot \lambda \nabla T + \text{internal sources and sinks} = C_p \rho \frac{dT}{dt}, \tag{1}$$

where λ is the thermal conductivity, C_p is the specific heat at constant pressure, and ρ the density. If there are no internal sources and sinks,

$$\nabla \cdot \lambda \nabla T = C_p \rho \frac{dT}{dt}. \tag{2}$$

For homogeneous materials whose thermal conductivity is nearly independent of temperature, we may treat λ as a constant. Then $\nabla \cdot \lambda \nabla T$ becomes $\lambda \nabla^2 T$ and equation (2) can be written as

$$\lambda \nabla^2 T = C_p \rho \frac{dT}{dt}, \tag{3}$$

or

$$\nabla^2 T = \frac{C_p \rho}{\lambda} = \frac{1}{a} \frac{dT}{dt}, \tag{4}$$

where $a = \lambda / C_p \rho$ is the thermal diffusivity.

For one-dimensional heat flow

$$a \frac{d^2 T}{dx^2} = \frac{dT}{dt}. \tag{5}$$

For heterogeneous materials, λ is not independent of position and λ should not be moved from behind the Dell operator [Eq. (2) to Eq. (3)]. In principle, then, the concept of diffusivity is inapplicable to heterogeneous materials. However, in practice, materials are never homogeneous as point defects, dislocations, grain boundaries, voids, etc., are present even in so-called homogeneous materials. Yet diffusivity techniques have been successfully applied to these materials for more than a century. Deliberate

attempts to extend diffusivity techniques to obviously heterogeneous materials have been made for many years. These efforts have been intensified since 1960's due to the development of the flash method for measuring diffusivity because of the relatively simple sample geometry, rapidity of measurements, and ease of handling materials with a large range of diffusivity values over large temperature intervals with a single apparatus.

The flash method, in which the front face of a small disc-shaped sample is subjected to a short laser burst and the resulting rear face temperature rise is recorded, is used in over 80% of the present thermal diffusivity measurements throughout the world. A highly developed apparatus exists at TPRL and we have been involved in an extensive program to evaluate the technique and broaden its uses. The apparatus consists of a Korad K2 laser, a high vacuum system including a bell jar window for viewing the sample, a tantalum tube heater surrounding a sample holding assembly, a spring-loaded thermocouple and IR detector, appropriate biasing circuits, amplifiers, A-D converters, crystal clocks, and a minicomputer-based digital data acquisition system capable of accurately taking data in the 40 microsecond and longer time domain. The computer controls the experiment, collects the data, calculates the results, and compares the raw data with the theoretical model.

The flash method has now been applied very successfully to composites consisting of a second phase more-or-less randomly dispersed in a continuous matrix [1,2] and also to composite materials composed of homogeneous layers sandwiched together [3,4].

A third class of composite materials is composed of fiber reinforcements imbedded in a more-or-less homogeneous matrix. Such composites are becoming increasingly important in new technological applications. One major sub-group of this class of composites are known as carbon/carbon materials. Carbon/carbon materials consist of arrays of graphite fibers lined up in one direction imbedded in a matrix consisting of arrays of graphite fibers lined up in more-or-less perpendicular directions with the spaces filled with graphite. A variety of geometries have been fabricated including 1-D, 2-D, 3-D and multidimensional arrays depending on the orientation of the fibers. These composites are being used in an increasing number of applications [5], at

least some of which involve transient heating conditions. It is therefore of interest to examine the response of such heterogeneous composites to transient heat fluxes.

The graphite fibers have high thermal conductivity/diffusivity values while the matrix materials have relatively low values compared to those of the fibers. Thus the fibers oriented in the direction of heat flow act as preferred paths for heat transfer. When such composites are subjected to an instantaneous heat pulse on one surface, the temperature wave is not planar. The results of thermal diffusivity methods and the applicability of the concept of diffusivity for such materials legitimately can be questioned. A preliminary study [6] on a coarse-weave 3-D carbon/carbon composite has shown that the normalized rear face temperature response curve following a laser pulse did not follow the theoretical pattern for homogeneous materials. However, the response curve for a fine-weave 3-D carbon/carbon material followed the theoretical curve very closely [7].

A detailed experimental study of thermal diffusion along the principal axes in an AVCO radially-pierced fabric^{TM} carbon/carbon material (HEPN-1) has been performed recently [8]. This work was supplemented by computer-aided analysis of thermal diffusion in HEPN-1 by J. Jortner (included as an appendix in Reference 8.) HEPN-1 can be considered to be a 2-D carbon/carbon material. From the combined results of the study on HEPN-1 and the previous research [6,7], the important parameters governing the results of a particular diffusivity experiment can be delineated. These parameters are listed in Table 1.

TABLE 1

Parameters Affecting Thermal Diffusivity Experiments

1. Magnitude of diffusivity of fibers and of matrix.
2. Fiber fraction ratio in direction of heat flow.
3. Thickness of sample in relation to fiber bundle spacing.
4. Rear face temperature sampling area and location.

Furthermore, from these experiments, it has been shown that:

(1) It is possible to measure diffusivity values which correspond to thermal conductivity values by using a sufficiently thick sample and large viewing area. The sample thickness required becomes less as the temperature is increased.

(2) It is possible to measure in-situ diffusivity values of fibers and of matrix by using point source temperature sensors and thin samples.

(3) It is possible to determine the effects of imperfections such as delaminations on the thermal diffusivity. These effects are manifest by matrix values lower than those for regions where the defects are not present (point source detector methods) and by an increase in diffusivity values for artifacts measured in gaseous environments as opposed to vacuum.

The present study was undertaken to further examine the use of the flash diffusivity technique for coarse-weave carbon/carbons. This study consisted of measuring the diffusivity of a variety of samples machined from on billet of 3-D carbon/carbon including measurements along the principal axes and at 45° to the principal axes, intercomparing the resultss and examining the expected rear face temperature rise curves based on finite element techniques.

II. SAMPLE DESCRIPTION

A piece of carbon/carbon from billet F-11, from the 7-inch Mantech program [9] was used as the sample material. The piece was from Ring No. 17 near the outside diameter in the forward part of the billet [10]. The dimensions were 5.8 cm in the axial direction, 1.8 cm in the radial direction and 2.3 cm in the circumferential direction. Thermal diffusivity samples were machined in the axial, (z) radial (r) and circumferential (θ) directions. In addition, samples were machined at 45° between the radial and axial directions (rz) and at 45° between the axial and circumferential directions (zθ). The nomenclature and directions tested as shown in Figure 1 (also included in Appendix I). The sample dimensions, masses and bulk density values are listed in Table 2. Measured unit cell dimensions and calculated

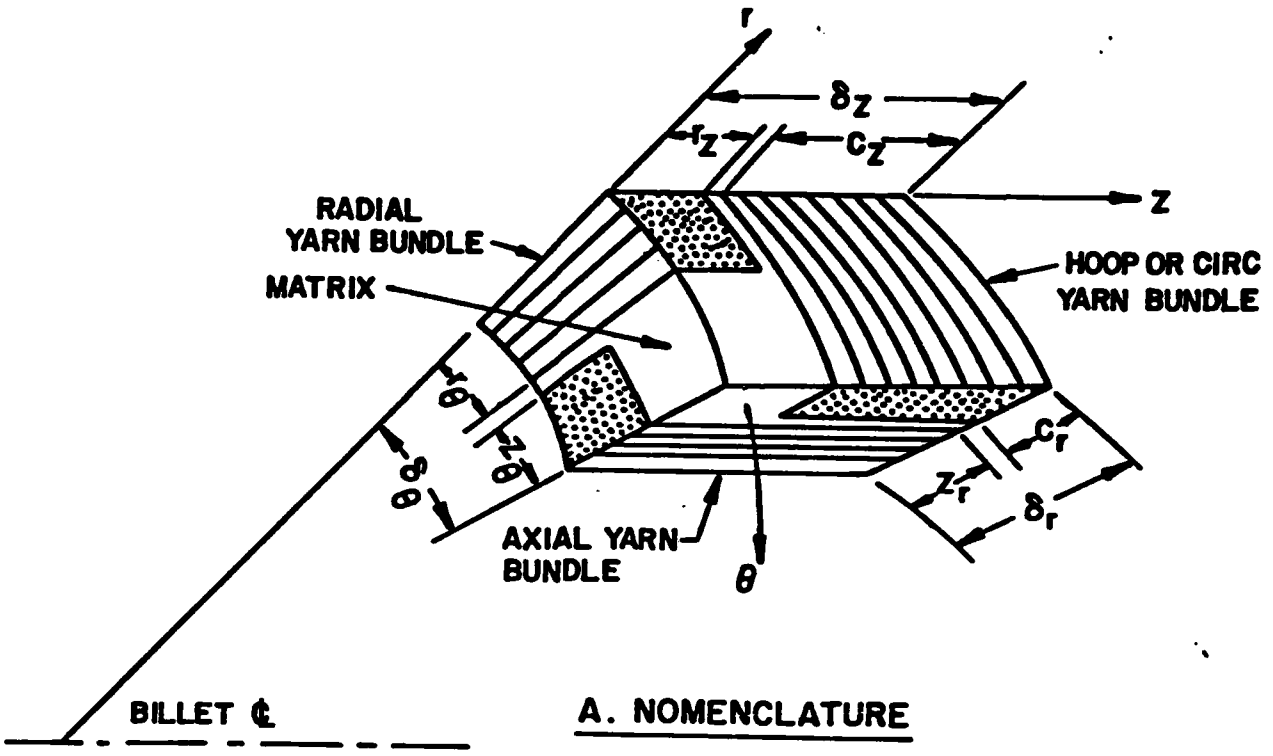

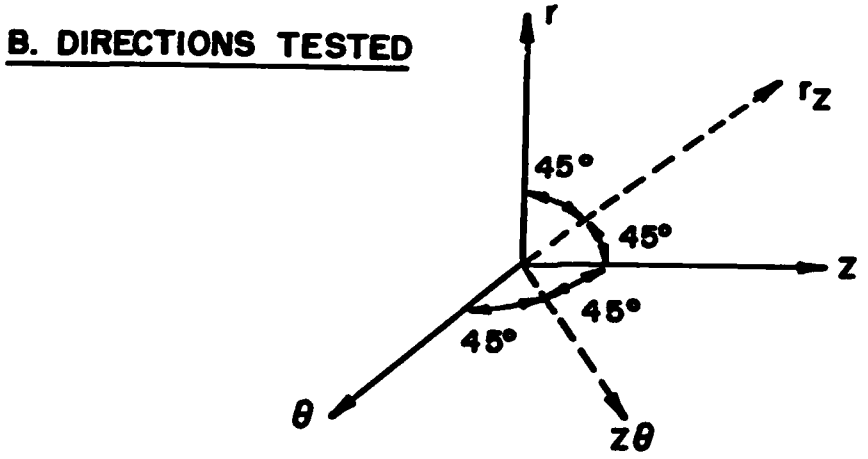

Figure 1. Nomenclature for 3-D Cylindrical Unit Cell and Sketch Showing Five Directions in Which Diffusivity was Measured.

TABLE 2

BULK DENSITY VALUES

SAMPLE (NO.)	THICK (IN.)	WIDTH (IN.)	WIDTH (IN.)	MASS (GMS)	DENSITY (GMS CM^{-3})
Axial	0.3008	0.4728	0.5000	2.2308	1.914
Radial	0.2628	0.4990	0.5004	2.0430	1.900
Circumferential	0.2998	0.4906	0.5009	2.3017	1.907
Axial-Circumferential	0.3010	0.4993*	--	1.8672	1.934
Axial-Radial	0.2990	0.5000*	--	1.8590	1.932

* Diameter

yarn bundle fractions for the principal axes are given in Table 3 (Table 1 of Appendix I). Thus the actual yarn bundle fractions in the axial, radial and circumferential directions for these samples are 0.195, 0.067 and 0.277, respectively.

Energy Materials Testing Laboratory measured the thermal diffusivity of axial and radial samples from the forward and aft sections of Rings 17 and 18 from billet F-11. These samples are listed in Table 4.

III. RESULTS

Thermal diffusivity results were obtained on the samples listed in Table 2 over the temperature range from about 100 to 1000°C. For each data set, diffusivity values were calculated at 10, 20, 25, 30, 33 $^{1}/_{3}$, 40, 50, 60, 66 $^{2}/_{3}$, 70, 75, 80 and 90% of the rear face temperature rise. The rear face temperature rise was one to two degrees Celsius. For homogeneous materials the diffusivity values calculated at these various percentage rises would all fall within a ±2% band. However, for materials with preferred heat diffusion paths, the diffusivity values calculated at various percent rises decrease with increasing percent rise. The magnitude of this increase is determined by the parameters listed in Table 1. In order to indicate the magnitude of the change in diffusivity values with increasing percent rise, diffusivity values calculated at 20, 50 and 80 percent rise times are given in Table 5. These results are plotted in Figure 2. From Table 5 and Figure 2, the following observations are made:

1. The diffusivity values for the circumferential, axial-circumferential and axial-radial samples are relatively independent of percent rise at all temperatures.

2. The diffusivity values for the axial sample, especially those calculated from 50 to 80%, become relatively independent of percent rise above 200°C.

3. The diffusivity values for the radial sample decrease rapidly with increasing percentage rise, especially at the lower temperatures and between 20 and 50%.

TABLE 3

Measured Unit Cell Dimensions (mm) and Calculated Yarn Bundle Fractions for On-Yarn Diffusivity Specimens from O.D. Region of Billet F-11

	Radial Sample	Axial Sample	Circ Sample
r_z	.41	-	-
r_θ	.81	-	-
z_r	-	.84	-
z_θ	-	1.67	-
C_r	-	-	1.07
C_z	-	-	.97
δ_r	-	2.18	2.29
δ_z	1.63	-	1.63
$\delta\theta$	3.05	3.30	-
V_f	.067	.195	.277

1. Dimensions listed are averages of several measurements made on polished surface of the specimen with a calibrated-eyepiece microscope at 20X magnification.

2. Yarn bundle fractions calculated using relations of this type:

$$V_r = \frac{r_z\, r_\theta}{\delta_z\, \delta_\theta}$$

TABLE 4

Energy Materials Testing Laboratory Diffusivity Samples†

EMTL SAMPLE (NO.)	SAMPLE (NO.)	DIRECTION	RING (NO.)	LOCATION	DENSITY* ($gm\ cm^{-3}$)	FIBER FRACTION** (SAMPLE)	FIBER FRACTION (VIEWING AREA)
F-11-F-5-OT-R-18-D-1	R-1	Radial	17	forward	1.9168	0.060	0.093
F-11-F-5-OB-R-18-D-2	R-2	Radial	18	aft	1.9281	0.060	0.020
F-11-F-5-OT-A-18-D-1	Ax-1	Axial	17	forward	1.9148	0.175	0.360
F-11-F-5-OB-A-18-D-2	Ax-2	Axial	18	aft	1.8919	0.175	0.160

† OD, Billett F-11

* density prior to measurement

** Preform values

TABLE 5

THERMAL DIFFUSIVITY RESULTS

SAMPLE	TEMP. (°C)	DIFFUSIVITY VALUE AT 20%	50%	80%
Axial	126	0.690	0.560	0.545
	277	0.503	0.386	0.366
	475	0.375	0.284	0.269
	640	0.333	0.249	0.234
	804	0.289	0.211	0.199
	960	0.191	0.177	0.187
Radial	121	0.530	0.437	0.368
	308	0.344	0.274	0.229
	468	0.261	0.211	0.183
	647	0.216	0.174	0.154
	831	0.178	0.146	0.134
	997	0.159	0.135	0.123
	1150	0.146	0.126	0.118
Circumferential	102	0.869	0.830	0.818
	213	0.680	0.624	0.602
	424	0.438	0.407	0.395
	641	0.339	0.320	0.313
	822	0.287	0.272	0.269
	1012	0.263	0.242	0.241
	1198	0.233	0.225	0.230
Axial-Circumferential	103	0.627	0.627	0.612
	233	0.449	0.450	0.449
	367	0.345	0.340	0.330
	552	0.268	0.261	0.261
	691	0.232	0.229	0.228
Axial-Radial	97	0.526	0.502	0.507
	165	0.362	0.350	0.330
	321	0.264	0.258	0.251
	495	0.215	0.202	0.199
	656	0.170	0.168	0.175
	730	0.166	0.160	0.163

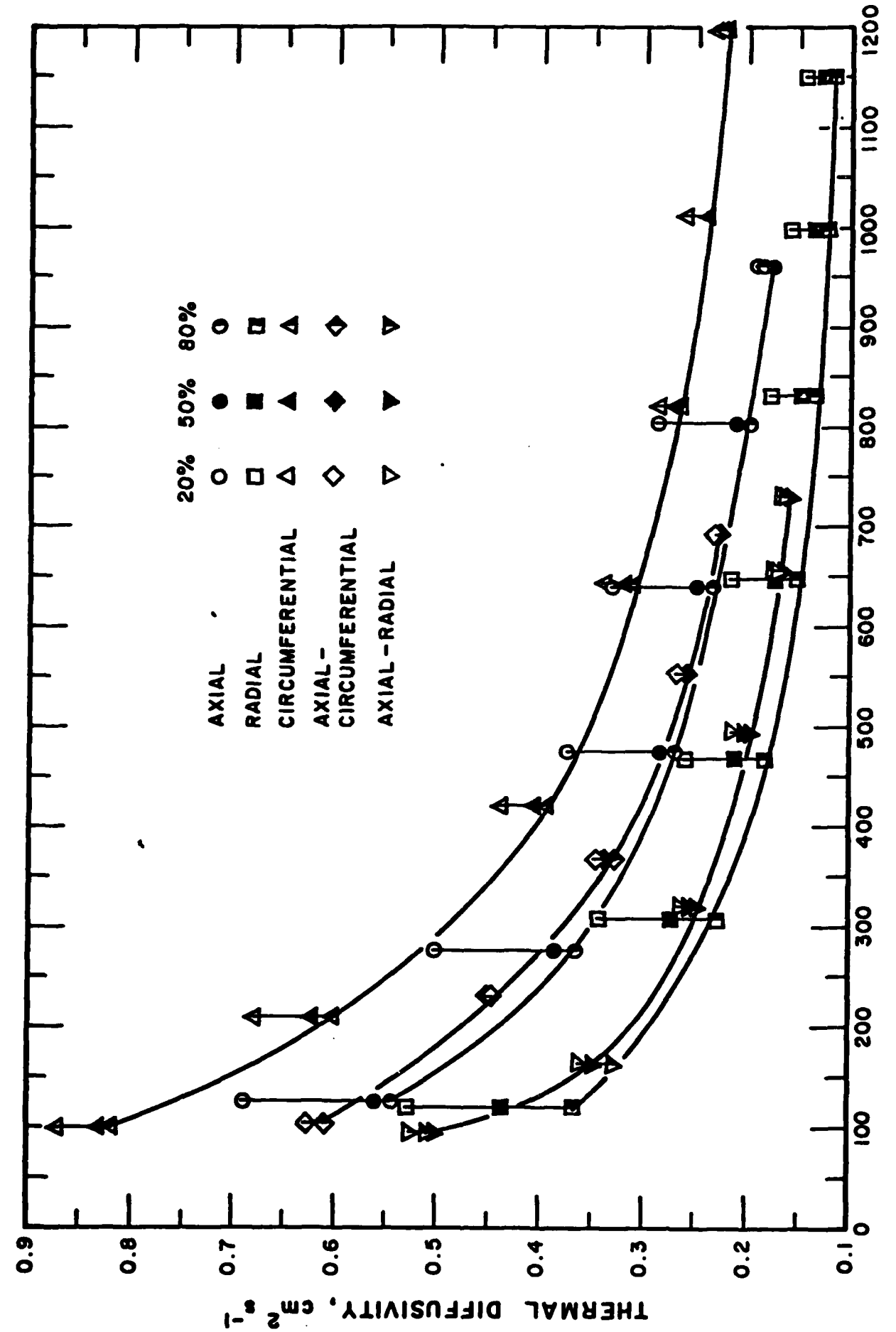

FIGURE 2. THERMAL DIFFUSIVITY RESULTS

In fact, the rear face temperature rise curves for the off-axis samples followed the theoretical models very well. This is illustrated in Figure 3 which shows the comparison between the theoretical model and the actual experimental data for the axial-circumferential sample at 552°C. Thus unambiguous diffusivity values are obtained for the off-axis samples and, as will be shown later, this will permit the development of a technique to obtain unambiguous on-axis diffusivity values.

In order to further explore the diffusivity values in the axial direction, a second sample was machined. This sample, here after identified as Axial 2 was 0.5 inches thick compared to only 0.3 inches thick for the axial sample. The diffusivity values measured on Axial 2 are given in Table 6. Since these results are similar to those obtained for the other axial sample, they are not shown in Figure 2. In addition to the diffusivity values obtained using an IR detector, diffusivity values were measured on Axial-2 using a point source thermocouple. The thermocouple locations in relation to fiber bundle positions are illustrated in Figure 4. The diffusivity values calculated at 20, 50 and 80% rise times at these positions are given in Table 7. Positions 1, 2 and 6 were partially on axial fiber bundles, while 3, 4 and 5 were mainly on transverse fibers. In particular the diffusivity values for positions 2 and 6 were higher than those for the other positions, especially at lower percent rise times. At the longer rise times, all the diffusivity values are much closer together. In fact the spread in diffusivity values is 250% at 20% rise and only 35% at 80% rise. The longer rise time values agree well with the value extrapolated to 23°C from the higher-temperature IR detector data (Tables 2 and 6).

In one experiment, the thermocouple was well-centered on an axial fiber bundle. The results are given in Table 8. The experimental rise curve data closely followed the theoretical model and the diffusivity values were all in the range from 2.71 to 2.83 cm^2 sec^{-1} from 20 to 80% rise. These values correspond to the in-situ fiber bundle at 23°C.

The diffusivity values reported by EMTL for their axial and radial samples are given in Table 9. These values were calculated at 50% rise times. The EMTL results for the axial samples are compared to the present results in Figure 5 and for the radial samples in Figure 6. For both types of samples, the present results parallel the EMTL results but are substantially larger.

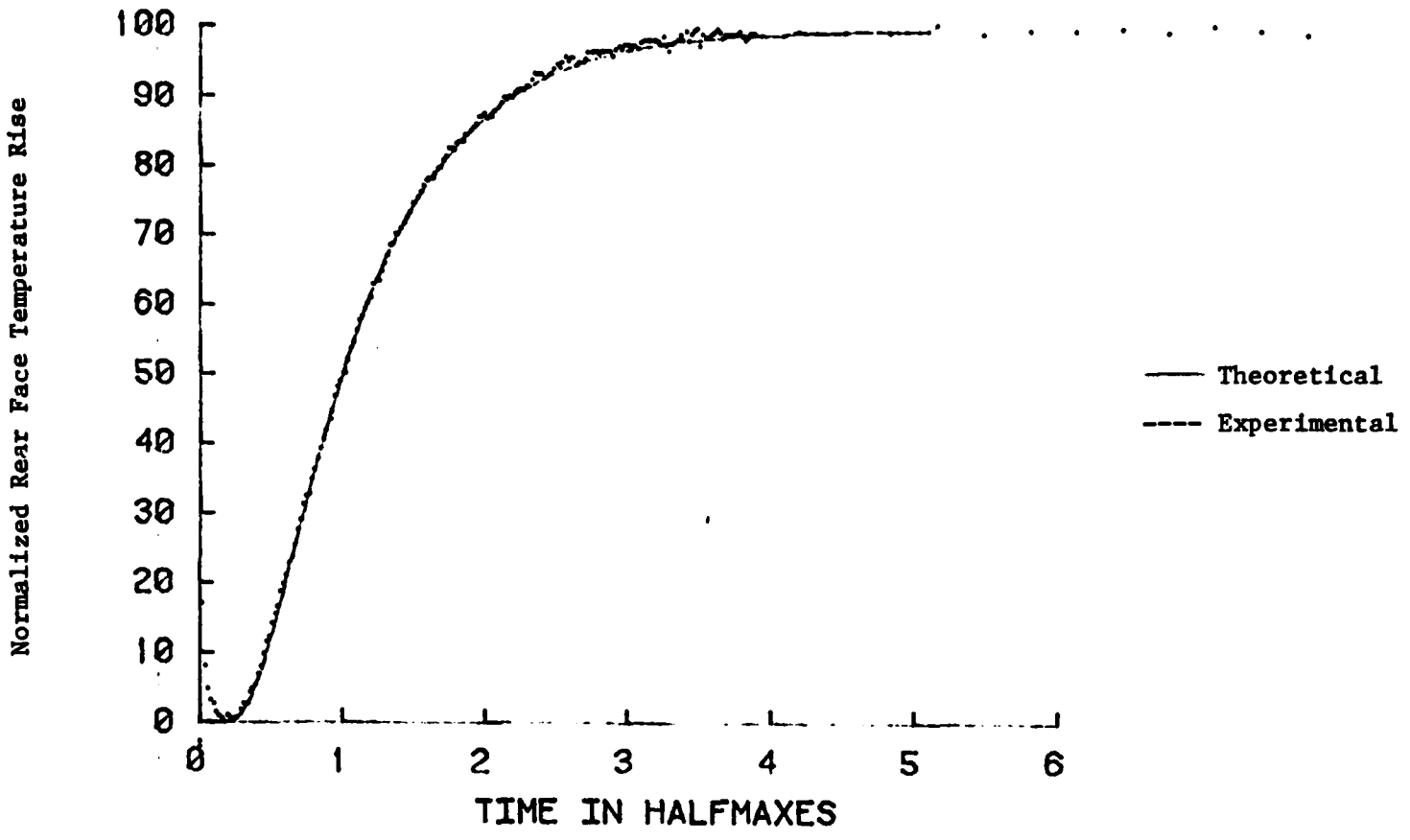

FIGURE 3. NORMALIZED REAR FACE TEMPERATURE RISE FOR AXIAL-CIRCUMFERENTIAL SAMPLE AT 552°C.

TABLE 6

THERMAL DIFFUSIVITY RESULTS

(Axial 2)

TEMP. (°C)	DIFFUSIVITY RESULTS AT 20%	50%	80%
94	0.637	0.614	0.607
220	0.519	0.437	0.416
306	0.415	0.345	0.321
414	0.326	0.296	0.293
520	0.314	0.276	0.271

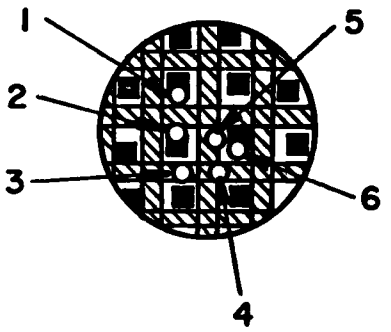

Figure 4. Location of Point-Source Temperature Sensing Probe (Axial-2 Sample).

TABLE 7

DIFFUSIVITY VALUES AS A FUNCTION OF POSITION

(Axial-2 Sample, 23°C)

POSITION (NO.)	CALCULATED DIFFUSIVITY AT 20%	50%	80%
1	1.418	1.042	0.925
2	2.252	1.678	1.153
3	1.210	1.005	0.958
4	0.879	0.775	0.782
5	1.017	0.892	0.828
6	2.104	1.401	0.978

TABLE 8

THERMAL DIFFUSIVITY VALUES FOR A FIBER BUNDLE EXPERIMENT

THERMAL DIFFUSIVITY

23C

	VALUE	TIME(SEC)
BASELINE:	0.94000	0.020680
HALFMAX:	3.46995	0.020033
MAXIMUM:	5.99990	0.073100

ALPHA	PERCENT	VALUE	TIME(SEC)
2.68307	10.0	1.44599	0.009761
2.74091	20.0	1.95198	0.012177
2.75494	25.0	2.20498	0.013333
2.74287	30.0	2.45797	0.014618
2.72871	33.3	2.62663	0.015530
2.71593	40.0	2.96396	0.017351
2.74435	50.0	3.46995	0.020033
2.71226	60.0	3.97594	0.023696
2.74445	66.7	4.31327	0.026136
2.79052	70.0	4.48193	0.027239
2.82674	75.0	4.73493	0.029499
2.78000	80.0	4.98792	0.033231
2.82117	90.0	5.49391	0.042620

FINITE PULSE TIME CORRECTION

2.809385	25.0
2.776830	50.0
2.848231	75.0

TABLE 9

DIFFUSIVITY RESULTS (EMTL)

EMTL SAMPLE (NO.)	SAMPLE (NO.)	TEMP. (°C)	DIFFUSIVITY (cm^{-2} sec^{-1})
F-11-F-5-OT-R-18-D-1	R-1	25	0.515
		49	0.475
		99	0.392
		154	0.320
		253	0.244
		355	0.191
		456	0.161
		553	0.137
		703	0.120
		854	0.104
		1000	0.094
F-11-F-5-OB-R-18-D-2	R-2	24	0.534
		50	0.460
		102	0.359
		151	0.308
		255	0.230
		351	0.183
		451	0.153
		555	0.132
		704	0.110
		851	0.097
		995	0.088
F-11-F-5-OT-A-18-D-1	Ax-1	25	0.653
		55	0.593
		104	0.513
		157	0.441
		256	0.327
		353	0.255
		451	0.210
		555	0.178
		698	0.153
		848	0.136
		988	0.127
F-11-F-5-OB-A-18-D-2	Ax-2	23	0.786
		50	0.682
		99	0.531
		152	0.444
		249	0.346
		349	0.273
		451	0.223
		550	0.196
		647	0.180
		749	0.160
		886	0.143
		992	0.136

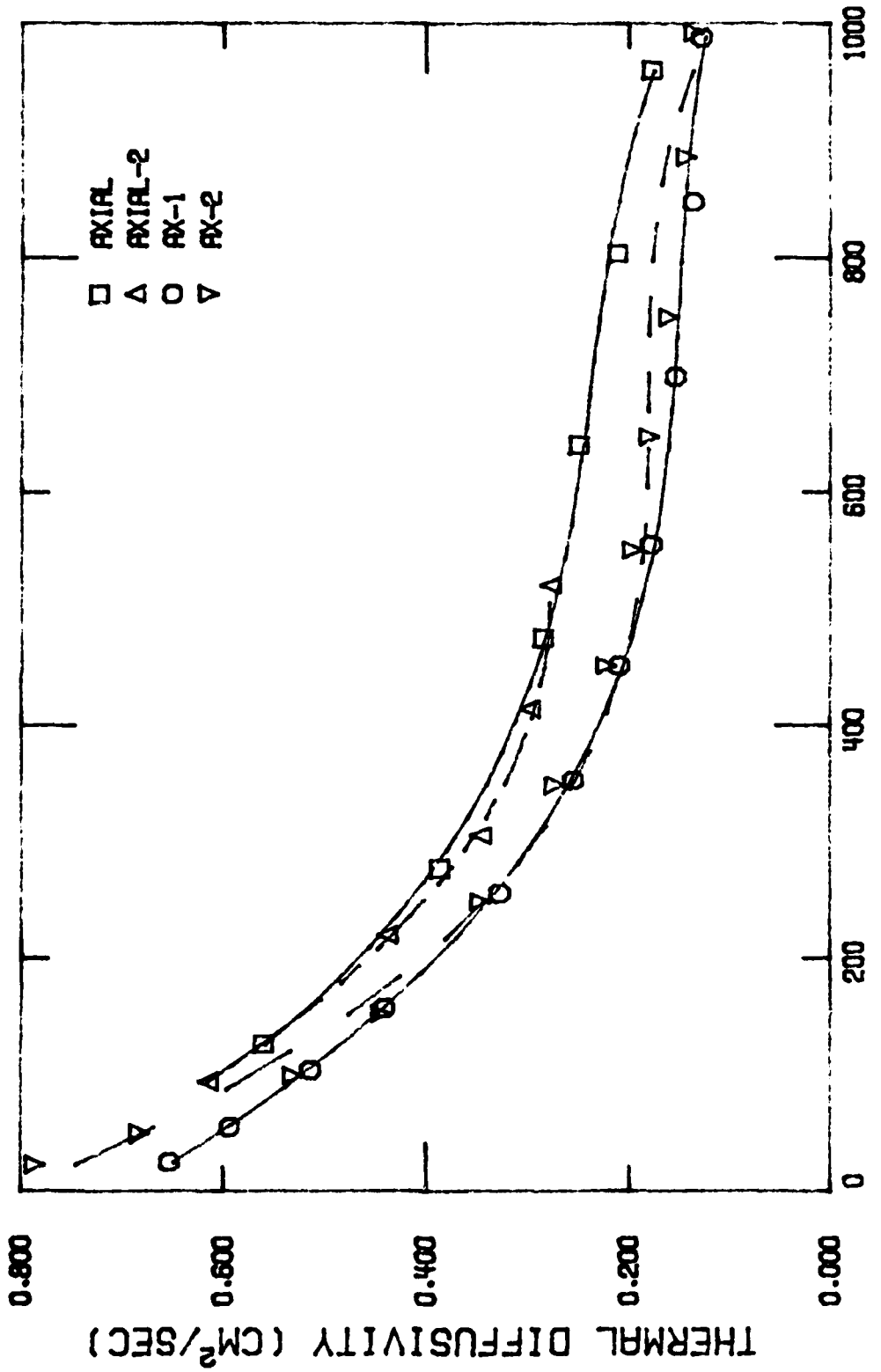

Figure 5. Comparison of EMTL and TPRL Diffusivity Results for Axial Samples.

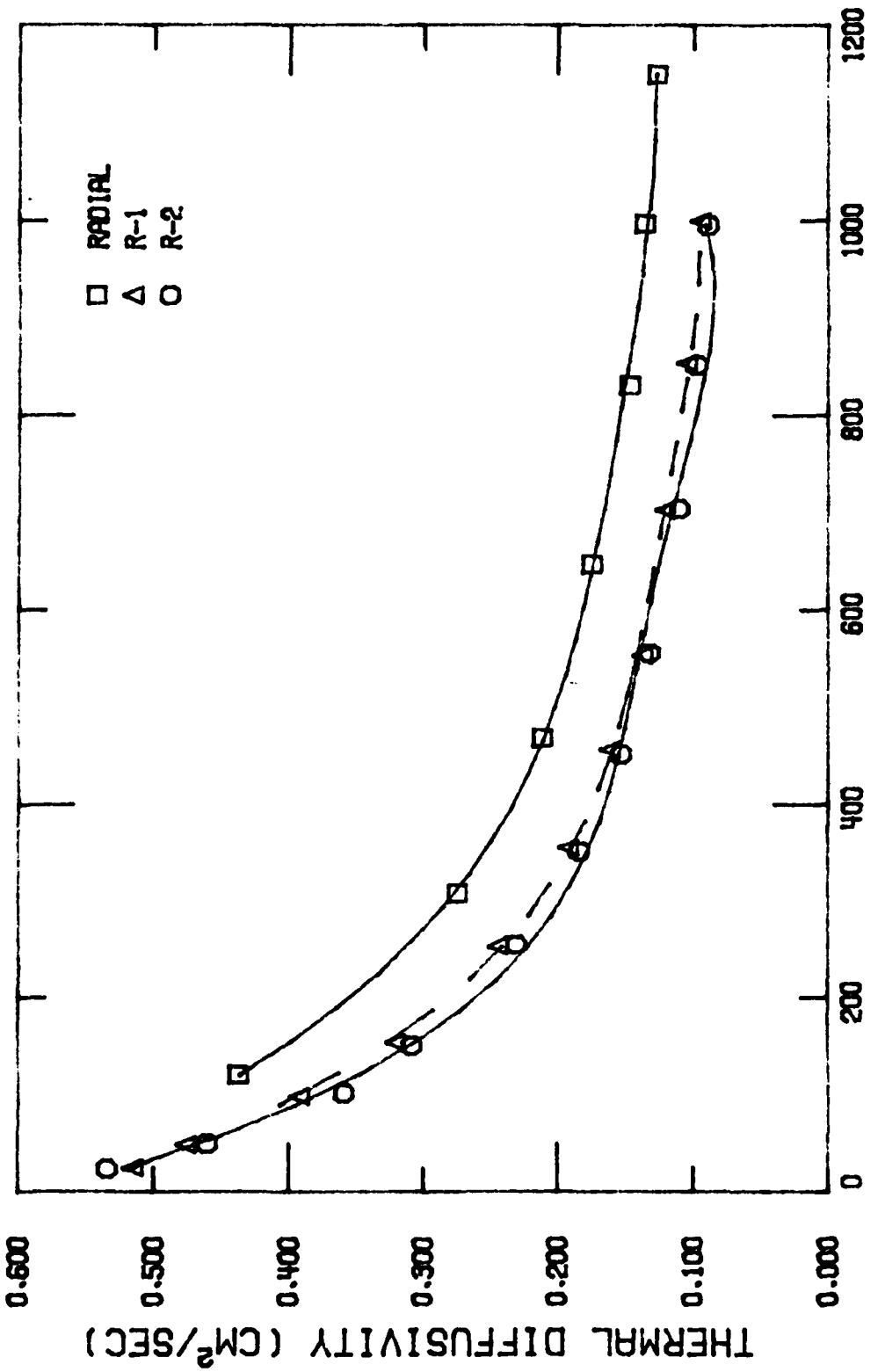

Figure 6. Comparison of EMTL and TPRL Diffusivity Results for Radial Samples.

IV. DISCUSSION

It has been shown that the diffusivity values calculated at the higher percentage rise times (longer experimental times) approach or equal the diffusivity values corresponding to conductivity (steady state) experiments. Using this as the basis "best" diffusivity values for the five sets of experiments are listed at selected temperatures in Table 10. These values are plotted in Figure 7. Using Equation (g) of Appendix I, namely $k_{nn} = 1/2(k_i + k_j)$, values for the 45° off-axis directions were calculated from the on-axis values of Table 10. These calculated values are compared to the experimental values for the two curves measured-namely axial-circumferential and axial-radial in Table 11. In general, the agreement was within 10%. When we consider the fact that the off-axis samples were not machined according to the recommended geometry (Figure 8, Appendix I), all the yarn bundles in the back face viewing area were not directly heated at the front face and this should lead to lower experimental values for the off-axis samples. From Table 11, it is noted that the experimental values are in fact lower than the calculated values with only one exception (axial-radial at 100°C).

"Steady-State" diffusivity values for 100, 200, 500 and 1000°C are plotted as a function of fiber fraction in the direction of heat flow in Figure 8. The solid lines represent the fiber fractions given in Table 3, (Case I) and the diffusivity values of Table 10 and Figure 7. The dashed lines in Figure 8 represent the situation in which the average fiber fraction value of 6.7% for the radial samples is replaced by 3.5% (Case II). Deshpande, and Bogaard, and Taylor [11] have shown that the fiber fraction in the IR detector viewing area may be substantially different than that for the over all sample average, especially for radial samples. Since the actual viewing area of our IR detector is not known accurately, we wished to examine the effects caused by the uncertainty of the actual fiber fraction in the viewing area. The diffusivity values obtained by extrapolating the solid lines [Case I] and dashed lines [Case II] to 0 and 100% are plotted as a function of temperature in Figures 9 and 10, respectively. These values correspond to those for the matrix (Figure 9) and for the fiber bundle (Figure 10).

TABLE 10

"STEADY STATE" THERMAL DIFFUSIVITY[+] RESULTS

TEMP. (°C)	SAMPLE DESIGNATION - AXIAL	RADIAL	CIRCUMFERENTIAL	AXIAL-CIRCUMFERENTIAL	AXIAL-RADIAL
100	0.570	0.352	0.803	0.607	0.478
200	0.408	0.266	0.621	0.479	0.313
300	0.333	0.216	0.483	0.381	0.262
400	0.284	0.182	0.401	0.314	0.222
500	0.252	0.158	0.350	0.275	0.195
600	0.228	0.143	0.315	0.248	0.174
700	0.210	0.131	0.291	0.226	0.157
800	0.196	0.122	0.270	0.211	0.147
900	0.185	0.115	0.255	0.200	0.136
1000	0.175	0.109	0.242	0.192	0.126

[+] $cm^2\ sec^{-1}$

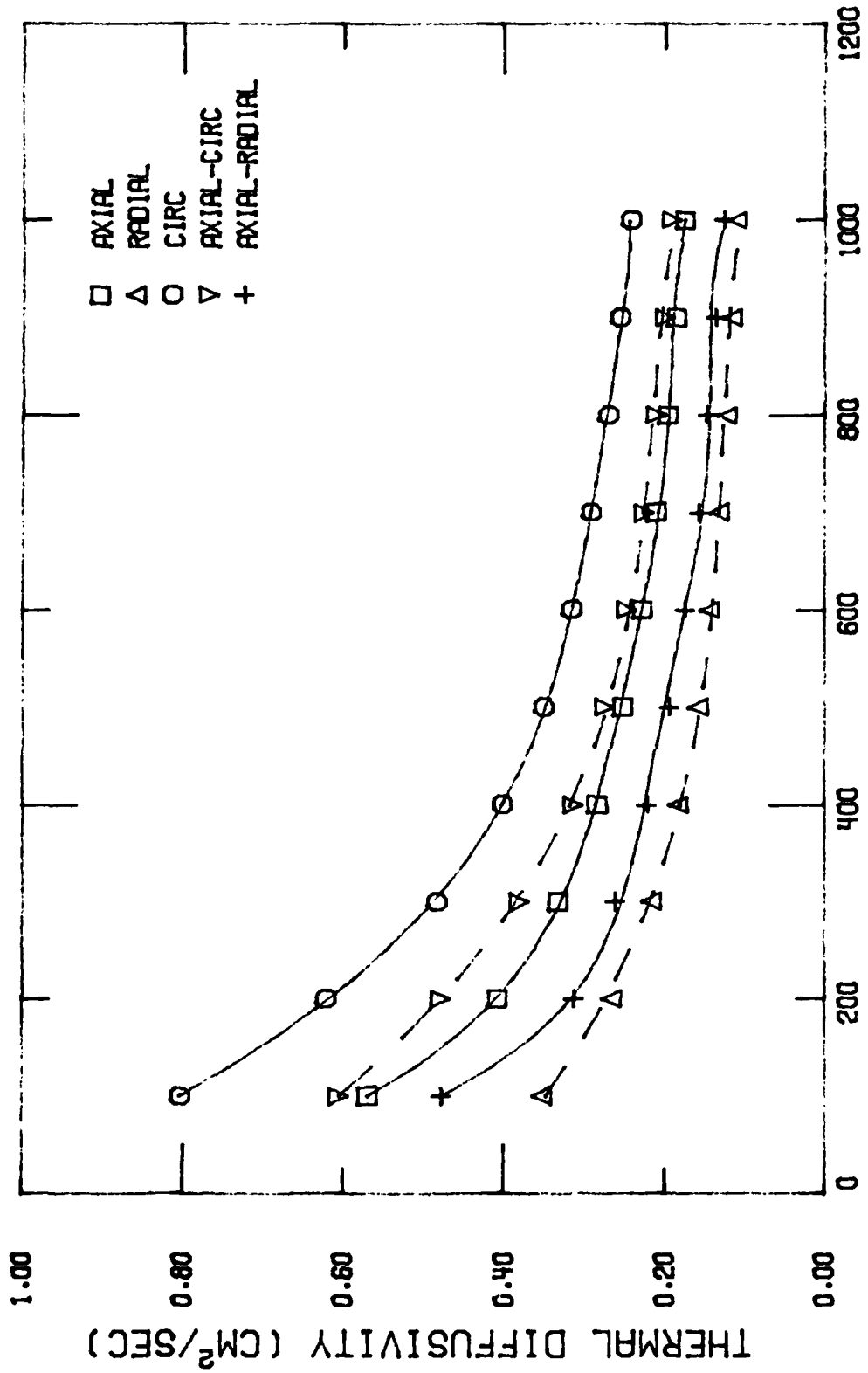

Figure 7. "Steady State" Diffusivity Values.

TABLE 11

CALCULATED AND MEASURED 45° OFF-AXIS DIFFUSIVITY VALUES

TEMP (°C)	AXIAL-CIRCUMFERENTIAL		AXIAL-RADIAL		RADIAL-CIRCUMFERENTI
	MEASURED	CALCULATED	MEASURED	CALCULATED	CALCULATED
100	0.607	0.687	0.478	0.461	0.578
200	0.479	0.515	0.313	0.337	0.444
300	0.381	0.408	0.262	0.275	0.350
400	0.314	0.343	0.222	0.233	0.292
500	0.275	0.301	0.195	0.205	0.254
600	0.248	0.272	0.174	0.186	0.229
700	0.226	0.251	0.157	0.171	0.211
800	0.211	0.233	0.147	0.159	0.196
900	0.200	0.220	0.136	0.150	0.185
1000	0.192	0.209	0.126	0.142	0.176

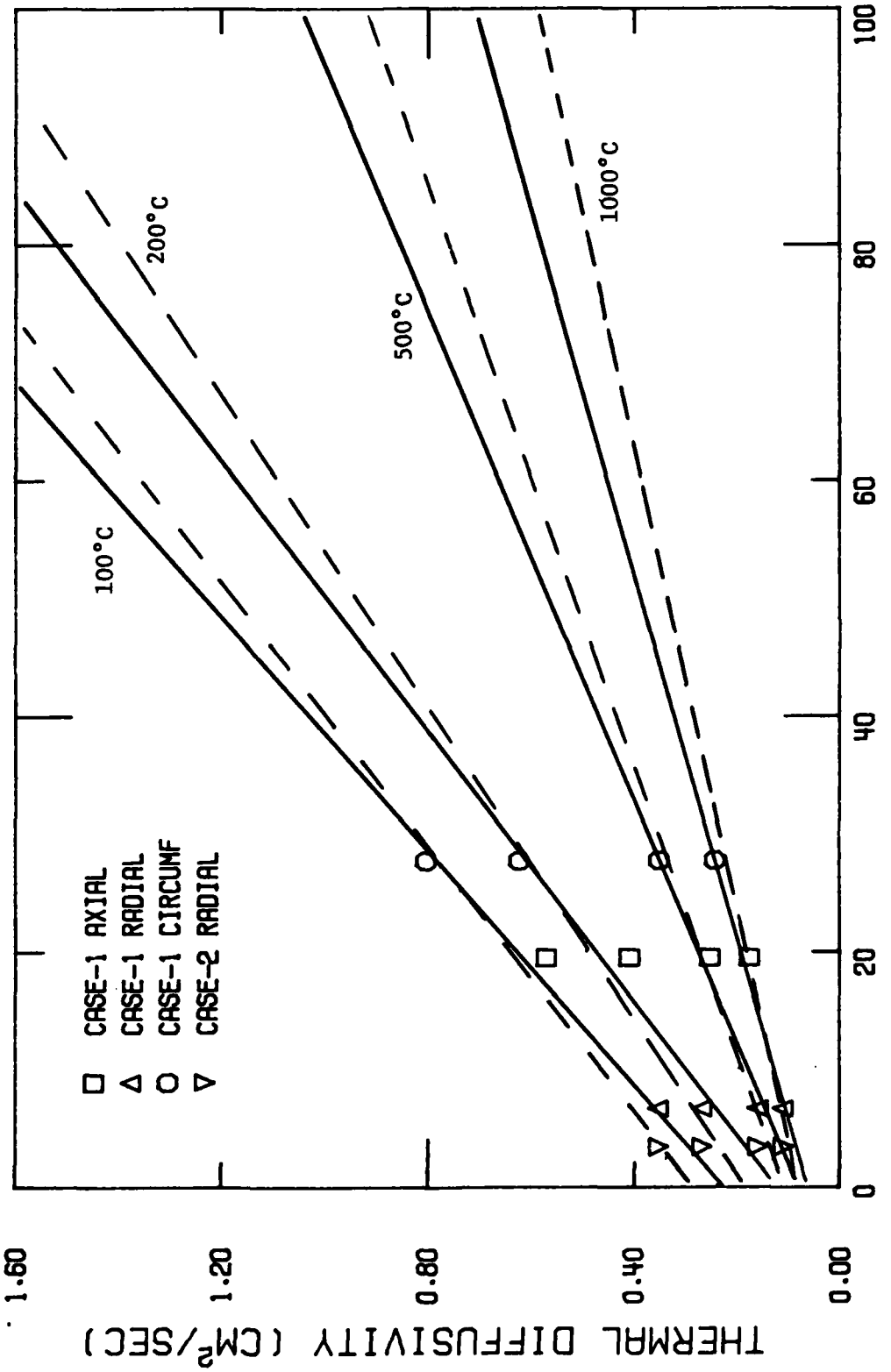

Figure 8. "Steady-State" Diffusivity Values Versus Fiber Fraction in Direction of Measurement.

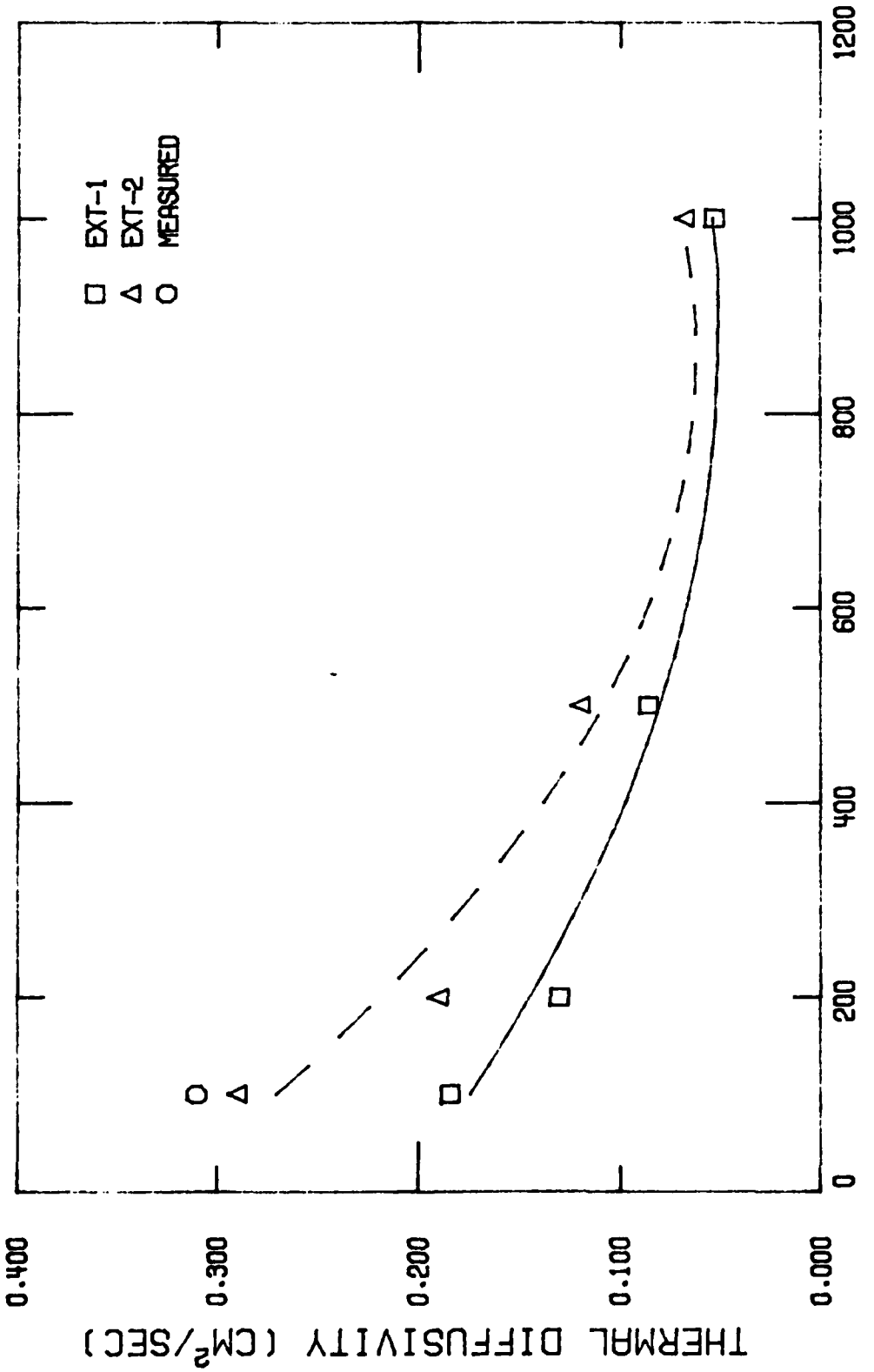

Figure 9. Thermal Diffusivity of the Matrix as a Function of Temperature.

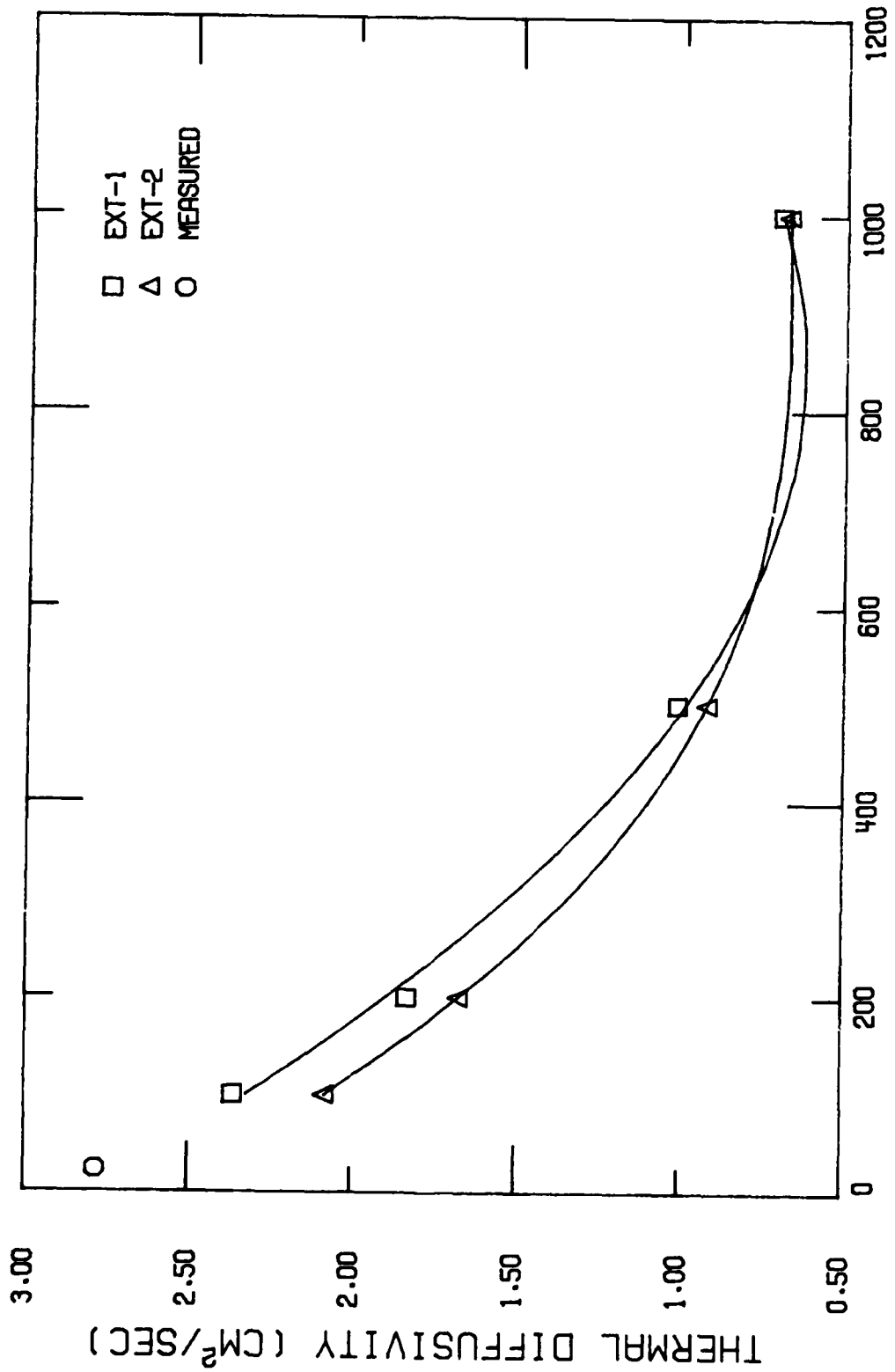

Figure 10. Thermal Diffusivity of the Fiber Bundles as a Function of Temperature

It was found possible to remove most of the axial fiber bundles from Sample Axial 2 and to replace them with matrix. Temperature rise curves measured in the resulting sample tended to follow the theoretical model fairly closely and a diffusivity value of 0.32 cm^2 sec^{-1} was obtained at 110°C in air. This is close to the Case II value, but is not in good agreement with the Case I results (Figure 9). Attempts were also made to determine the effects of slight displacement of the radial sample at 100°C. The results for those displacements were 0.398, 0.429, 0.390 at the 50% rise times measured in air. This variation is too small to permit a large error in the fiber-fraction assigned to the IR viewing area. However, two interesting observations were made during these tests; namely that the diffusivity values were noticeably lower and less dependent on percent rise time than the values recorded initially (Table 5 and Figure 2), and the diffusivity values were noticeably lower when measured in vacuum. The diffusivity values measured in air and calculated at 80 and 90% rise times were less than 10% below the 50% rise time values when measured in air. The radial sample had been sent to J. Jortner for microscopic examination and this procedure included sample polishing. If we substitute the "Steady-State" diffusivity values measured on the polished sample, we would still be on the dashed line (Case II Figure 8) at least for the 100°C data. Thus it is possible that the diffusivity values measured on the matrix-only sample agrees with the diffusivity values obtained by extrapolating to 0% fiber-fraction.

Reasonable agreement was obtained between the diffusivity value measured for a fiber bundle (Table 8) and the diffusivity value extrapolated to 100% fiber-fraction for either the Case I or Case II situation (Figure 10).

The flash technique has been shown to be a powerful tool for studying transient heat flow in carbon/carbon materials. As a result of the present work, the following conclusions can be drawn:

1. Thermal diffusivity values measured on 45° off-axis samples yield unique values which define unambiguously the "steady-state" diffusivity values along the principal axes.

2. Diffusivity values measured along the principal axis, especially below 500°C in the axial and radial directions, depend upon sample thickness, detector viewing area, and percent rise time chosen to make the calculations. Nevertheless, it is possible to obtain diffusivity values equivalent to the steady state case.

3. It is possible to determine the diffusivity of the matrix and of the fiber bundles both by direct measurements and by extrapolating diffusivity values measured on samples containing various known fiber fractions in the direction of measurement to 0 and 100%, respectively.
4. It is possible to determine the diffusivity values for the matrix and fiber bundles as a function of temperature using the extrapolation method given in 3.
5. There is a surface layer in carbon/carbon in which inter-constituent temperature gradients are significant and beyond which they are negligible. The material may be treated as homogeneous for the purposes of heat conduction through parts which are much thicker than the heterogeneity dimension. However, within a surface layer subjected to large heat fluxes, the analysis must consider the heterogeneity.

Additional diffusivity work on carbon/carbon materials is warranted. Specifically such work should take into account certain deficiencies in the present study. These deficiencies include:

(1) Insufficient sample material for machining samples along all principal axes and all 45° off-axis directions
(2) Viewing area of IR detector and relation to fiber-bundle locations should be controlled
(3) Off-axis samples should be configured as shown in Figure 8 of Appendix I.
(4) Effects of handling samples, especially polishing, and the effects of gaseous environment should be investigated.

REFERENCES

1. Lee, H.J. and Taylor, R.E., "Determination of Thermophysical Properties of Layered Composites by Flash Method," Thermal Conductivity 14, Edited by P.G. Klemens and T.K. Chu (New York: Plenum Press), 423-34, 1976.

2. Lee, T.Y.R. and Taylor, R.E., "Thermal Diffusivity of Dispersed Materials," J. Heat Transfer, 100(4), 720-4, 1978.

3. Lee, T.Y.R., Donaldson, A.B., and Taylor, R.E., "Thermal Diffusivity of Layered Composites," Thermal Conductivity 15, Edited by V.V. Mirkovich (New York: Plenum Press), 135-48, 1978.

4. Taylor, R.E., "Heat-Pulse Thermal Diffusivity Measurements," High Temperatures - High Pressures, 11 43-58, 1978.

5. Fitzer, E. and Heym, M., "High -Temperature Mechanical Properties of Carbon and Graphite (A Review)," High Temperatures - High Pressures, 10, 29-66, 1978.

6. Taylor, R.E. and Groot, H., "The Thermophysical Properties of a Coarse Woven Carbon-Carbon Rocket Nozzle Material," TPRL 206R, February 1980.

7. Taylor, R.E., Groot, H., and Showmaker, R.L., "Thermophysical Properties of Fine Weave Carbon/Carbon Composites," presented at 16th AIAA Thermophysics Conference.

8. Taylor, R.E. and Groot, H., "Thermophysical Properties of a Carbon/Carbon Composite," TPRL 244, May 1981.

9. Ellis, R.A., "7-Inch Billet Program Progress Report," RNTS Meeting, 1979, CPIA Publication 310, January 1980.

10. Energy Materials Testing Laboratory, "Interim Report on Mechanical and Thermal Properties of Billet F-11 Seven Inch Mantech Billet Program Vol. II: Thermal Properties," MCIC No. 109500, March 1980.

11. Deshpande, M.S., Bogaard, R.H., and Taylor, R.E., "Variances In The Measurement of Thermal Diffusivity on Course Weave C-C Composites and the Dependence Upon Fiber-Fraction," International Journal of Thermophysics, 2 (4), 357-70, 1981.

ON THE USE OF OFF-AXIS TESTING TO CHARACTERIZE THE THERMAL DIFFUSIVITIES OF ORTHOGONALLY REINFORCED CARBON-CARBON COMPOSITES*

Julius Jortner
Science Applications, Inc.
Irvine, CA 92715

February 1982

Introduction and Summary

For coarse weave composites, significant errors can occur in interpreting diffusivity tests because of temperature differences among the variously oriented yarn bundles in the test specimen (eg, Reference 1). One manifestation of these errors is that the diffusivities calculated from the backface temperature traces in flash-method tests are significantly affected by the temperature rise-fraction used to reduce the data.

Previous efforts to measure the thermal diffusivities of 3D carbon-carbon composites have used samples oriented to measure the principal conductivities - that is, in the directions parallel to each of the three orthogonal sets of yarn bundles in the composite. This article describes some tests on a representative coarse weave composite in which data also were obtained in directions at appreciable angles to the yarns. The diffusivities inferred from these off-axis tests show less dependence on rise fraction, and appear, therefore, to be more reliable indicators of bulk composite behavior than the on-axis data. This finding leads to a recommendation that off-axis testing

* Acknowledgements
The interest and support of R.E. Taylor (Purdue University) are gratefully acknowledged. The research was sponsored by Air Force Office of Scientific Research under Contract F49620-81-C-0011 via a subcontract from Purdue University. Discussions with F.I. Clayton and W.C. Loomis, of SAI, were of beneficial influence on the work presented.

be included routinely in the characterization of 3D composites. However, because of the limited number of tests conducted in the effort described, further testing appears necessary to firmly establish the validity of the recommendation. In particular, the dependence of the off-axis data on specimen dimensions and proportions needs exploration.

Experimental Results

A piece of carbon-carbon billet F-11, from the 7-Inch Mantech program (Reference 2), was supplied to TPRL for the purpose of exploring the thermal diffusivity in a coarse-weave material. A schematic of the unit cell of a 3D cylindrical composite is shown in Figure 1. The piece, about 22 cubic centimeters in volume, was taken from the outer region of the billet where the yarn bundle fractions in each of the three principal directions are approximately (Table 1):

$$V_r = .067$$
$$V_z = .195$$
$$V_\theta = .277$$

Samples were excised at TPRL to measure diffusivity in each of five directions: the three "on-axis" directions, along the radial, axial, and circ yarn bundles; and in two "off-axis" directions, 45-degrees between the axial and radial directions, and 45-degrees between the axial and circ directions. These directions are illustrated in the lower half of Figure 1. The purpose of the 45-degrees off-axis tests was to provide data which would check the self-consistency of the diffusivity results, as the off-axis data is, in principle (Reference 3), predictable from the on-axis data.

The tests were by the flash-laser method, described in Reference 1, and the data were reduced at TPRL from the backface rise times corresponding to rise-fractions of 20, 50, and 80 percent. These results are listed in Table 2. The data have been plotted in Figures 2, 3, and 4 for rise-fractions of 20, 50, and 80 percent, respectively.

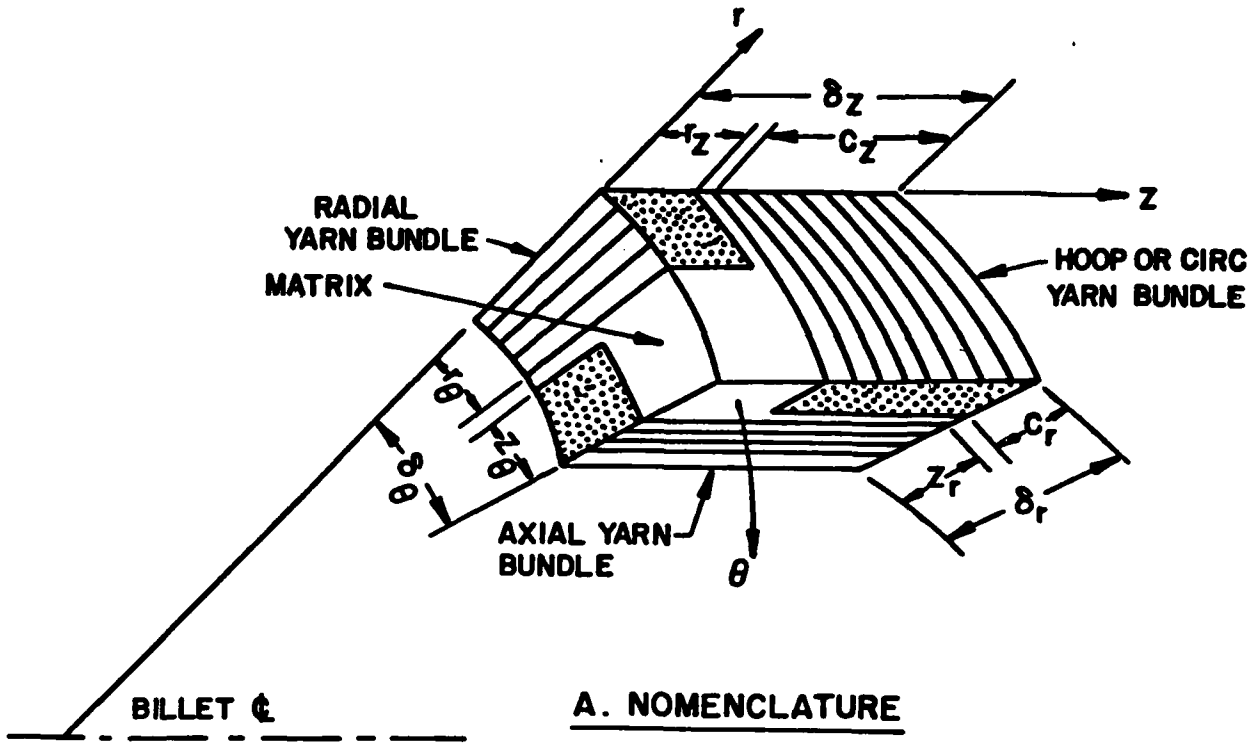

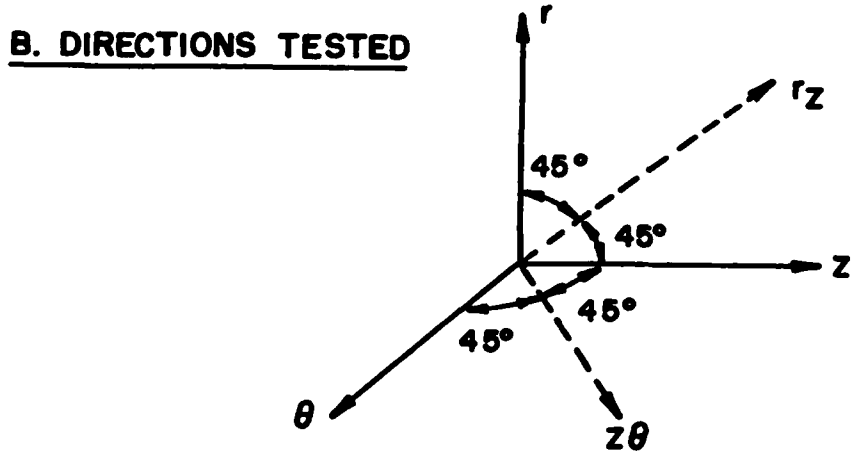

Figure 1. Nomenclature for 3D cylindrical Unit Cell and Sketch Showing Five Directions in which Diffusivity was Measured.

Table 1

Measured Unit Cell Dimensions (mm) and Calculated Yarn Bundle Volume Fractions for On-Yarn Diffusivity Specimens from O.D. Region of Billet F-11

	Radial Sample	Axial Sample	Circ Sample
r_z	.41	-	-
r_θ	.81	-	-
z_r	-	.84	-
z_θ	-	1.67	-
C_r	-	-	1.07
C_z	-	-	.97
δ_r	-	2.18	2.29
δ_z	1.63	-	1.63
δ_θ	3.05	3.30	-
V_i	.067	.195	.277

1) Dimensions listed are averages of several measurements made on polished surface of the specimen with a calibrated-eyepiece microscope at 20X magnification.

2) Yarn bundle volume fractions calculated using relations of this type:

$$V_r = \frac{r_z\, r_\theta}{\delta_z\, \delta_\theta}$$

TABLE 2

THERMAL DIFFUSIVITY RESULTS (cm^2/sec)

SAMPLE	TEMP. (°C)	DIFFUSIVITY VALUE AT 20%	50%	80%	RISE FRACTION EFFECT, %
Axial	124	0.627	0.542	0.508	23.4
	126	0.690	0.560	0.545	26.6
	277	0.503	0.386	0.366	37.4
	475	0.375	0.284	0.269	39.4
	640	0.333	0.249	0.234	42.3
	804	0.289	0.211	0.199	45.2
	960	0.191	0.177	0.187	2.1
Radial	121	0.530	0.437	0.368	44.0
	308	0.344	0.274	0.229	50.2
	468	0.261	0.211	0.183	42.6
	647	0.216	0.174	0.154	40.3
	831	0.178	0.146	0.134	32.8
	997	0.159	0.135	0.123	29.3
	1150	0.146	0.126	0.118	23.7
Circumferential	102	0.869	0.830	0.818	6.2
	213	0.680	0.624	0.602	13.0
	424	0.438	0.407	0.395	10.9
	641	0.339	0.320	0.313	8.3
	822	0.287	0.272	0.269	6.7
	1012	0.263	0.242	0.241	9.1
	1198	0.233	0.225	0.230	1.3
Axial-Circumferential	103	0.627	0.627	0.612	2.5
	233	0.449	0.450	0.449	0.0
	367	0.345	0.340	0.330	4.5
	552	0.268	0.261	0.261	2.6
	691	0.232	0.229	0.228	1.8
Axial-Radial	97	0.526	0.502	0.507	3.7
	165	0.362	0.350	0.330	9.7
	321	0.264	0.258	0.251	5.2
	495	0.215	0.202	0.199	8.0
	656	0.170	0.168	0.175	-2.9
	730	0.166	0.160	0.163	1.8

Rise fraction effect is defined as $\frac{\alpha_{20} - \alpha_{80}}{\alpha_{80}} \times 100$ percent, where α_{20} and α_{80} are the diffusivity values at 20- and 80-percent rise fraction respectively.

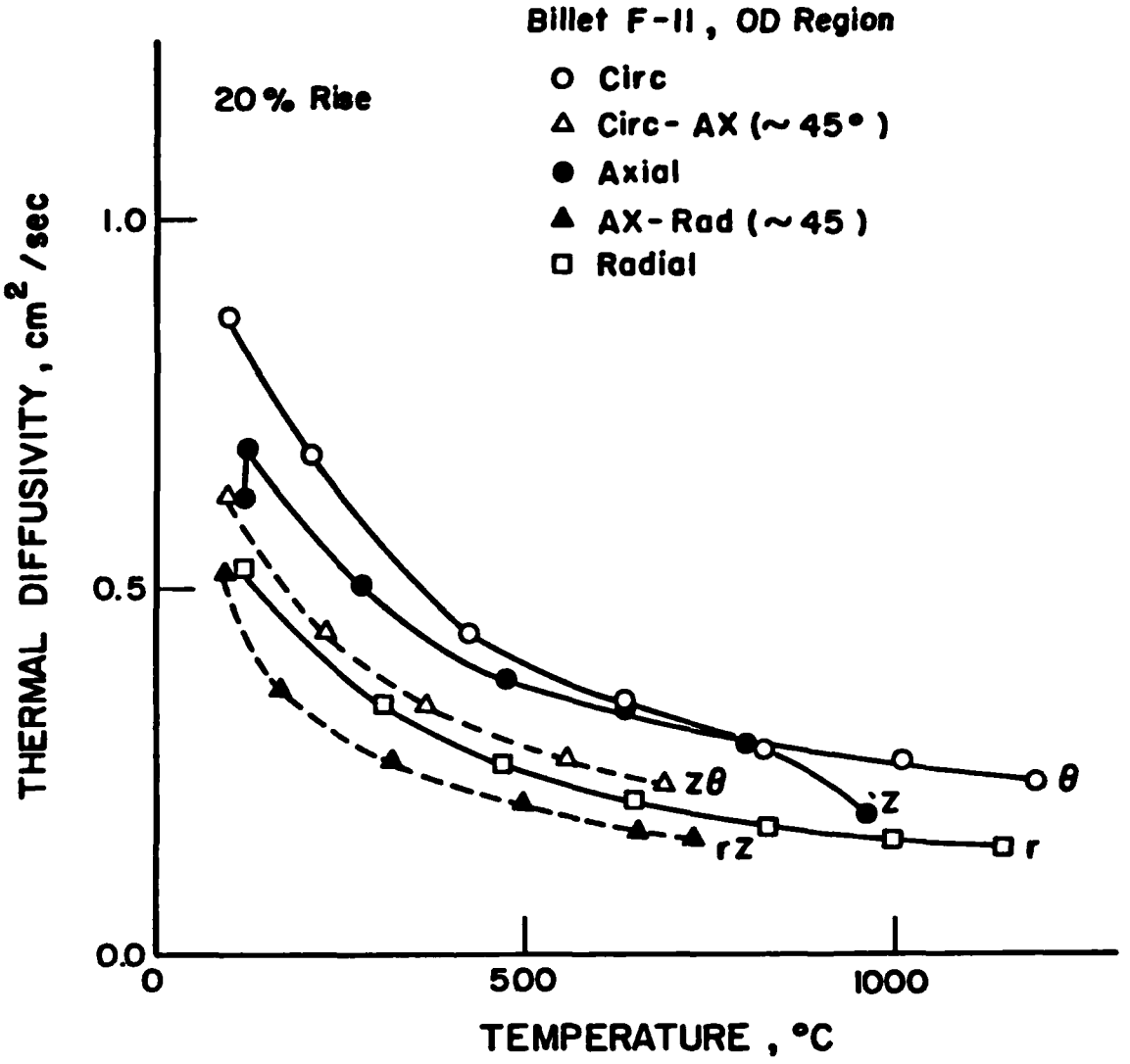

Figure 2. Thermal Diffusivities Inferred from 20% Rise-Fraction Data.

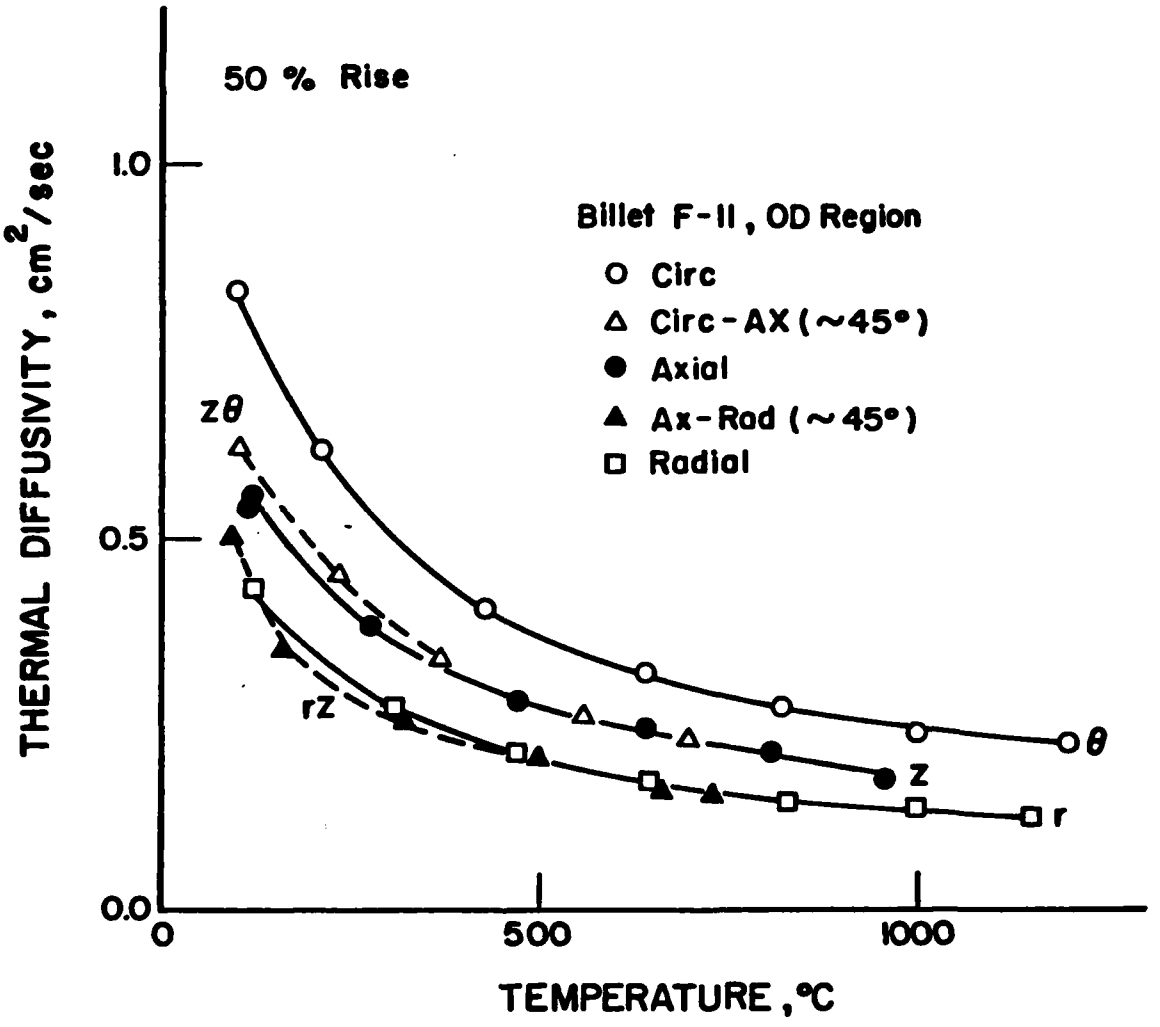

Figure 3. Thermal Diffusivities Inferred from 50% Rise-Fraction Data.

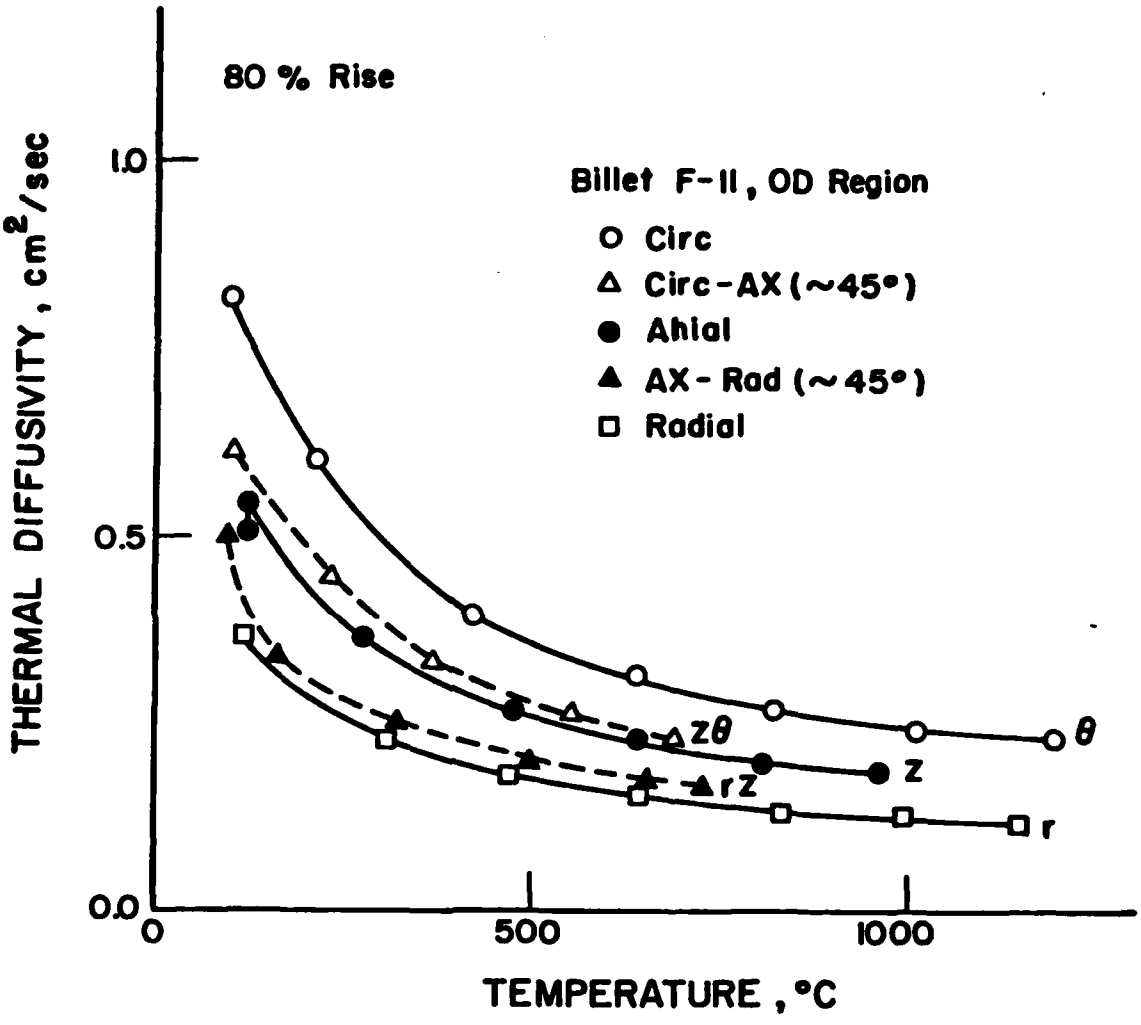

Figure 4. Thermal Diffusivities Inferred from 80% Rise-Fraction Data.

Analytical Relationships Between On-Axis and Off-Axis Conductivities

By definition, heat flux by conduction is related to thermal gradients by:

$$[-Q] = [K]\,[T'] \tag{a}$$

The matrix equation can be stated more fully as:

$$\begin{Bmatrix} -Q_i \\ -Q_j \\ -Q_k \end{Bmatrix} = \begin{bmatrix} K_{ii} & K_{ij} & K_{ik} \\ K_{ji} & K_{jj} & K_{jk} \\ K_{ki} & K_{kj} & K_{kk} \end{bmatrix} \begin{Bmatrix} T'_i \\ T'_j \\ T'_k \end{Bmatrix} \tag{b}$$

For an orthotropic material, when i, j, and k are the principal axes of the material (eg, r, z, and θ, in a cylindrical 3D composite):

$$\begin{Bmatrix} -Q_r \\ -Q_z \\ -Q_\theta \end{Bmatrix} = \begin{bmatrix} K_r & 0 & 0 \\ 0 & K_z & 0 \\ 0 & 0 & K_\theta \end{bmatrix} \begin{Bmatrix} T'_r \\ T'_z \\ T'_\theta \end{Bmatrix} \tag{c}$$

The principal conductivities, k_r, k_z, and k_θ, can be derived from on-axis tests diffusivity tests using the relationship:

$$[K] = c\rho\,[\alpha] \tag{d}$$

To derive the conductivity in an off-axis direction, n, from the principal conductivities, the rotation of the thermal conductivity tensor of equation (c) gives (Reference 3):

$$K_{nn} = l^2_{ni}\,K_i + l^2_{nj}K_j + l^2_{nk}\,K_k \tag{e}$$

For the simple case where n is in the plane normal to the k axis and ϕ_k is the angle between the n and the i axes:

$$K_{nn} = (K_i - K_j)\cos^2\phi_k + K_j \tag{f}$$

If ϕ_k is chosen as 45 degrees:

$$K_{nn} = \frac{1}{2}(K_i + K_j) \qquad (g)$$

Thus, we see that the conductivities measured in the off-axis tests should be bounded by the on-axis conductivities, and, when the angle is 45 degrees, the off-axis conductivity is the simple arithmetic average of the conductivities along the two neighboring principal axes.

Also, it turns out that three independent off-axis tests could be used to derive the full thermal conductivity tensor. For example, three equations, of the form of equation (g), can be solved simultaneously to yield:

$$\begin{aligned} K_r &= K_{\underline{rz}} + K_{\underline{r\theta}} - K_{\underline{\theta z}} \\ K_z &= K_{\underline{rz}} - K_{\underline{r\theta}} + K_{\underline{\theta z}} \\ K_\theta &= -K_{\underline{rz}} + K_{\underline{r\theta}} + K_{\underline{\theta z}} \end{aligned} \qquad (h)$$

where $K_{\underline{rz}}$ is the conductivity in the direction 45 degrees between the r and z yarns, and $K_{\underline{r\theta}}$ and $K_{\underline{\theta z}}$ are similarly defined.

Discussion of Results

The measurements in the directions of the yarns rank themselves in the expected order. That is, the diffusivity increases with increased yarn volume fraction. Figure 5, a cross-plot of the information in Figure 3, shows that the rise in diffusivity with fiber volume fraction is approximately linear. A linear relationship between thermal conductivity and yarn volume fraction:

$$K_i = A V_i + B$$

has been found to give good correlation with a wide range of data for 3D carbon-carbon composites (Reference 4).

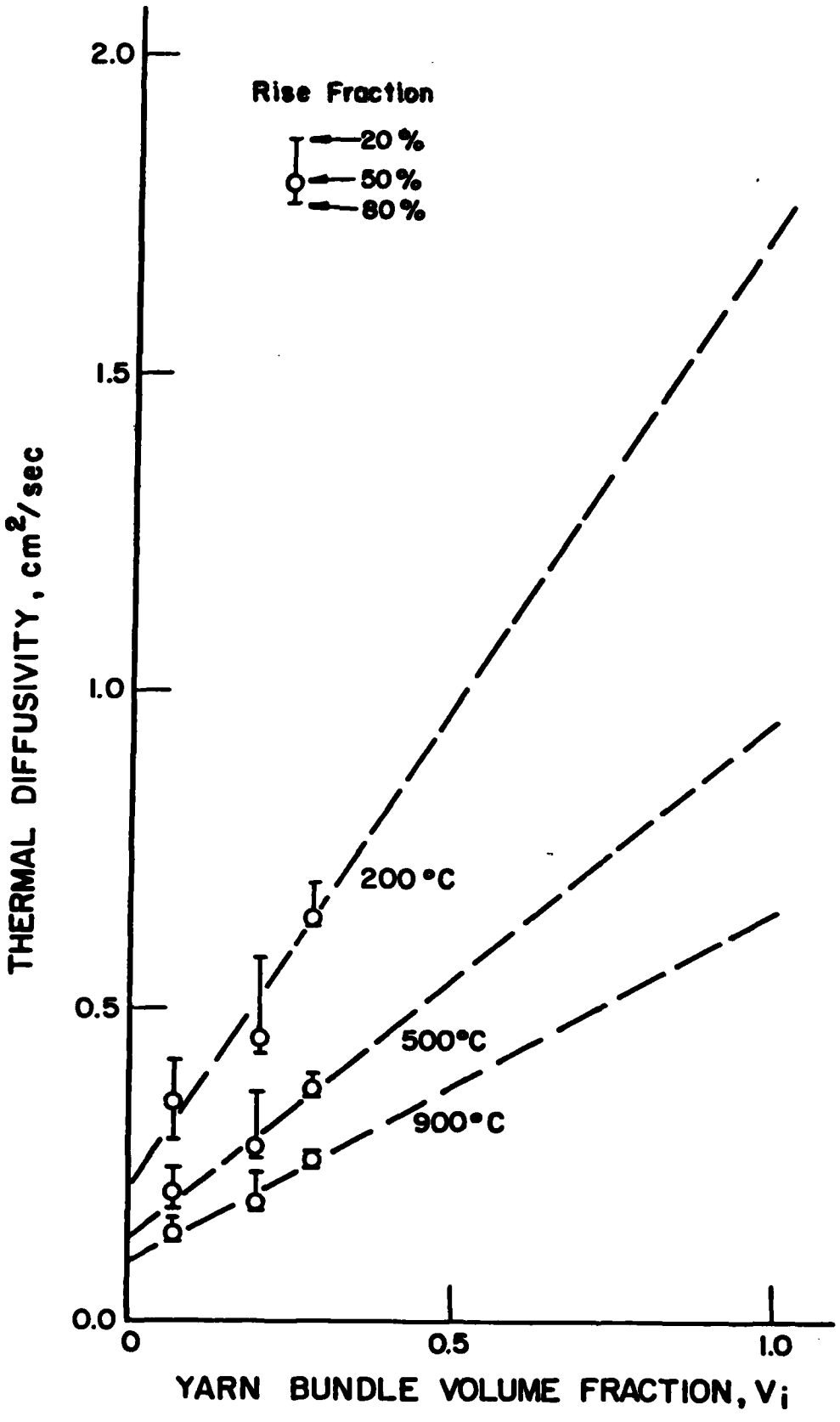

Figure 5. Trends of Diffusivity Vs. Volume Fraction of the Yarn Bundles in the Direction of Measurement.

Inspection of Table 2 shows that the effect of rise fraction on measured diffusivity is greatest in the radial and axial directions and least in the 45-degrees (off-axis) specimens. The reason probably is that the texture of the 45-degree surfaces is more "uniform" than the textures of the on-axis specimens. That is, more of the 45-degree surface represents yarn bundle sections (Figure 6); thus, the mean distance between high conductivity areas is smallest on the 45-degree surfaces, implying that the temperature gradients within these surfaces are smaller than within the on-axis surfaces.

This effect might be quantified in terms of the area fraction of yarn bundles at the front and backfaces of the specimen. Figure 7 shows how the rise-fraction effect (listed in the last column of Table 2) varies with yarn bundle area fraction. The trend line has been drawn with the aid of the two extreme points (at area fractions of zero and unity) that represent "homogeneous composites" for which the rise-fraction effect should be close to zero. The trend suggests that using three off-axis specimens, instead of three on-axis specimens, would provide more reliable estimates of bulk composite diffusivities.

As pointed out in the preceding section, complete characterization of the conductivity tensor of an orthogonally reinforced composite requires only three independently-oriented measurements. From these, the conductivity in any direction may be calculated. Thus the 45-degree measurements are, in principle, redundant. For a coarsely-textured composite, however, the 45-degree measurements (assuming they are more reliable than the on-axis measurements, as implied in the preceding paragraph) can serve as a check on the consistency of the data, via equation (g).

Comparing the off-axis results to the on-axis results, we see that data from the shorter rise-fractions (Figures 2 and 3) obviously are not self-consistent because the 45-degree diffusivities, are outside the ranges defined by the two relevant on-axis diffusivities. For the 80-percent rise fraction, the 45-degree results are between the relevant on-axis results, but somewhat

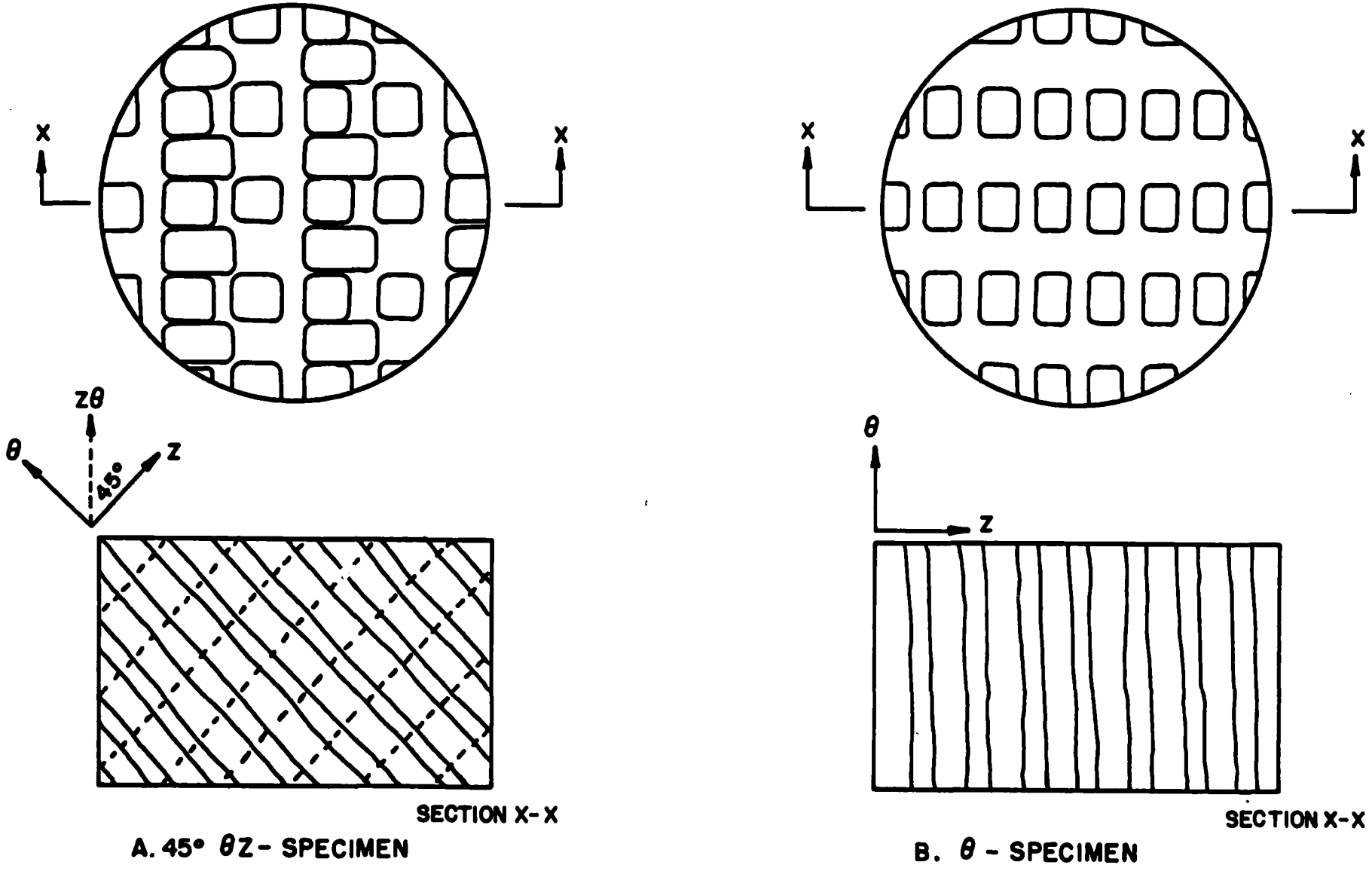

Figure 6. Comparison of Textures in the Off-Axis 45° θZ Specimen and the on-Axis θ-Specimen.

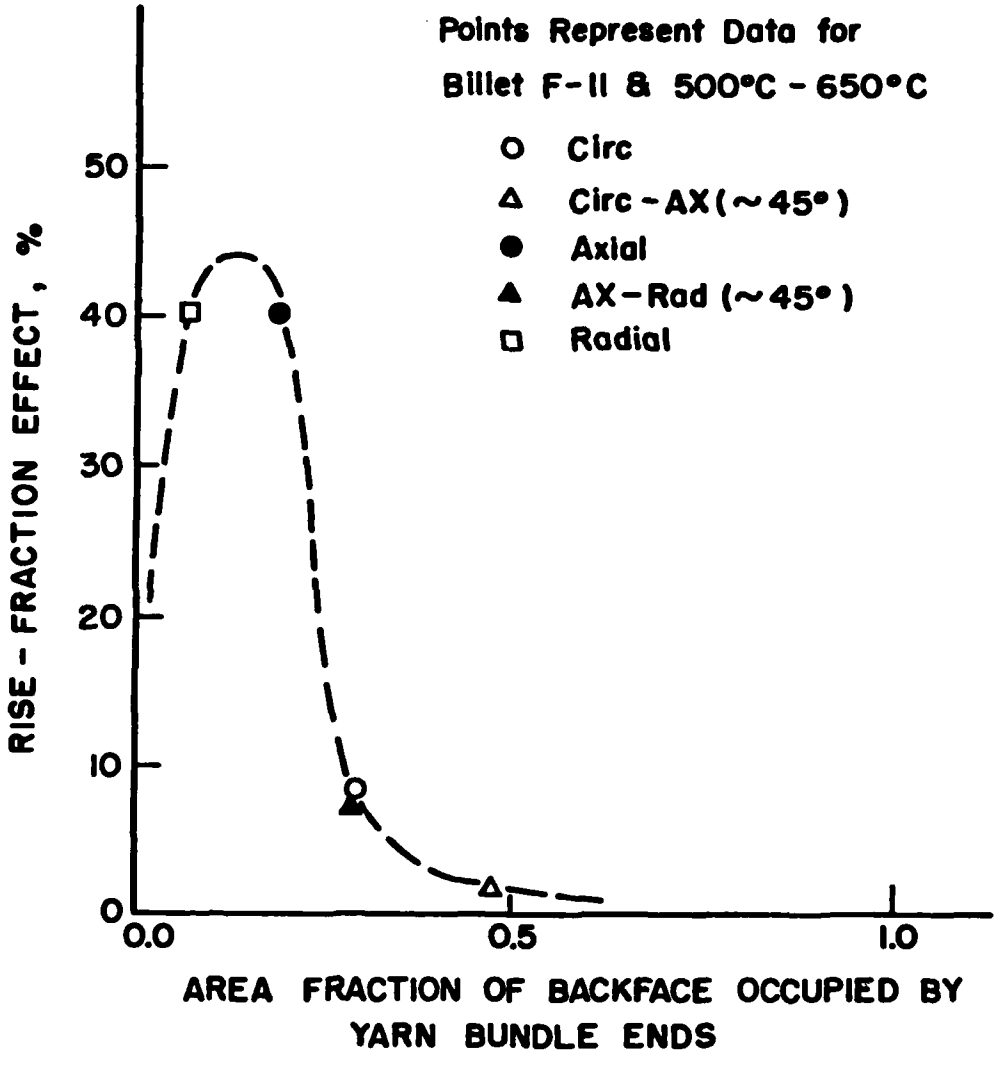

Figure 7. Effect of Yarn-Bundle Area Fraction on Magnitude of Rise-Fraction Effect.

lower than the mean value expected if the data were self-consistent and if the samples were properly cut at 45-degrees.

It should be noted that some data scatter will result from slight variations in unit-cell dimensions and yarn bundle volume fractions from specimen to specimen; for example, Table 1 shows variations of about 5% in unit cell dimensions δ_r and δ_θ for the specimens used here. Thus, perfect consistency is not to be expected for this variable material.

The relatively low values of the 45-degree off-axis diffusivities may be due, in part, to improper selection of the specimen proportions. Because the yarn bundles are the primary carriers of heat in the composite, it would be better to proportion the specimen as illustrated in Figure 8 so that all the yarns in the back face viewing area would be directly heated at the front face. Inspection of Figure 6 shows that such was not the case in the tests performed here. Because some of the yarns in the actual viewing area were heated only by conduction within the composite, it is likely that the resulting value of diffusivity is lower than would be obtained in a wider specimen.

Conclusions and Recommendations

The results described above support the conclusion that diffusivities derived from off-axis tests are less subject to errors, arising from temperature gradients within a coarse-textured composite specimen, than diffusivities derived from on-axis tests.

As off-axis tests can be used to characterize completely the conductivities of a 3D composite, we recommend that:

1) Off-axis tests be used, instead of on-axis tests, to characterize the conductivities of coarse-textured 3D composites.

2) The off-axis specimens be proportioned as shown in Figure 8.

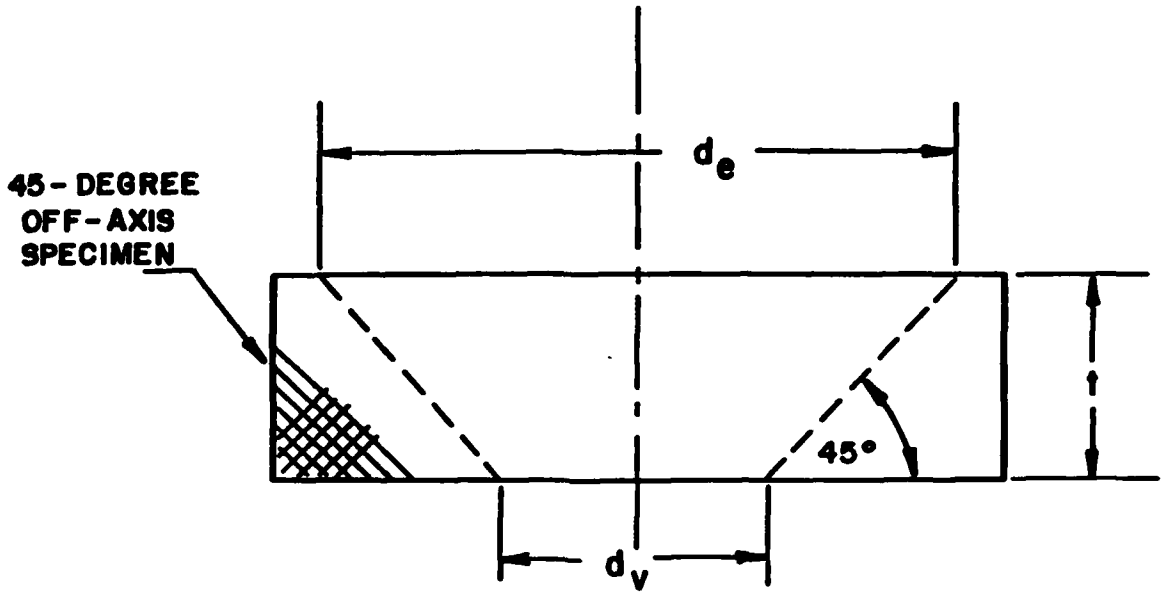

CRITERION: $d_e \geq d_v + 2t$

d_e = diameter of area exposed to laser

d_v = diameter of area of temperature measurement

Figure 8. Recommended Off-Axis Specimen Geometry

3) The actual angles at which the specimens are cut should be measured and equation (e) be used to infer the full conductivity tensor, instead of the simpler equation (g) which was used here for illustrative purposes.

Before the preceding recommendations are adopted, it would be prudent to do some more exploratory testing with emphasis on the effects of specimen geometry (Figure 8) on off-axis data.

References

1. R.E. Taylor and H. Groot, Thermophysical Properties of a Carbon-Carbon Composite, Special Report for AFOSR Grant 77-3280, Purdue University Report TPRL 244, May 1981.

2. R.A. Ellis, 7-Inch Billet Program Progress Report, RNTS Meeting, 1979, CPIA Publication 310, January 1980.

3. H.S. Carslaw and J.C. Jaeger, Conduction of Heat in Solids, 2nd Edition, see Chapter 1.20, Oxford, 1959.

4. F.I. Clayton and D.A. Eitman, Material Property Characterization Results for 7-Inch Carbon-Carbon Billet Program, 1980 JANNAF Propulsion Meeting, Monterey, March 1980.

Nomenclature

A, B	temperature-dependent constants
c	specific heat
i,j,k	orthogonal coordinates
l_{in}	cosine of the angle between the i and n vectors
K_i	thermal conductivity in the i-direction, a principal axis of the material
K_{ij}	thermal conductivity constant relating heat flow in the i-direction to a temperature gradient in the j-direction
Q_i	heat flux in the i-direction
r,θ,z	radial, circumferential, and axial directions in a cylindrically reinforced billet.
T'_i	temperature gradient in the i-direction,
v_i	volume fraction of yarn bundles parallel to the i-direction
x_i	distance along the i-direction
α_i, α_{ij}	thermal diffusivities, analogous to K_i and K_{ij}
ϕ_k	angle of rotation of coordinate system about the k axis
ρ	mass density

ANALYSIS OF TRANSIENT TEMPERATURE RESPONSE OF A CARBON-CARBON COMPOSITE DURING CONTINUOUS HEATING AT ONE SURFACE*

Julius Jortner
Science Applications, Inc.
Irvine, California 92715

February 1982

INTRODUCTION

The study reported earlier (Reference 1), on transient temperature responses of carbon-carbon composites during flash-diffusivity tests, has been continued to explore the effects of the composite's heterogeneity during situations in which the heating is continuous, as in a rocket motor firing.

In the previous study it was found that temperature gradients in thermal diffusivity specimens of carbon-carbon material can affect the diffusivity value derived from a flash test, and that increasing the axial length of the specimen decreases the errors that might occur from this cause. Although the average behavior of relatively large pieces of carbon-carbon was shown equivalent to the behavior of a homogeneous material having the same average diffusivity, concern was expressed that the interconstituent temperature gradients close to a heated surface may be significant to localized thermal processes such as ablation. This concern motivates the calculations reported here. That is, we ask how significant are the temperature gradients in a carbon-carbon composite that is heated continuously at one surface as in the case of a rocket motor throat insert.

* Acknowledgements
The heat transfer calculations were performed by T.C. Duncan, using the "TASC" computer code, developed at SAI and described in Reference 1. The interest and support of R. E. Taylor (Purdue University) are gratefully acknowledged. The research was sponsored by Air Force Office of Scientific Research under Contract F49620-81-C-0011 via a subcontract from Purdue University.

CASE ANALYZED

The same "TASC" computer program, described and used in the previous study (Reference 1), was applied to the same sort of axisymmetric idealization of the composite (Figure 1), using the same properties for the two constituents (Table 1). The case analyzed is schematically described in Figure 2; the mesh used in the analysis is shown in Figure 3.

The model represents a single yarn bundle and its proportionate share of surrounding material. The center-to-center spacing of the yarns in the composite is 0.24 cm and the diameter of the yarn bundles is 0.12 cm. The yarn bundle has a high conductivity along its length (the "axial" direction) and a low conductivity transverse to the length. The surrounding material has an intermediate (rather low) conductivity and is assumed isotropic. The composite is heated at the front face (at the top of the sketch in Figure 2) by radiation from a 3000°K source; the radiation exchange is assumed to occur with a view factor of unity and both the source and the composite have emmissivities of one. The composite is 2.5 cm thick (approximately one inch) and the back face radiates to a 300°K environment also with an emissivity of one. Initially, at time equals zero, the composite is at a uniform temperature of 300°K. Heating begins when the front face is suddenly exposed to the 3000°K source.

The use of radiative, rather than convective, heat input was merely a matter of convenience in using the TASC code. Although convection is probably the dominant mode in a rocket motor, we felt that the major aspects of inter-constituent temperature differences could be illustrated with the case analyzed. The numerical value of the coldwall heat flux (that is, the heat flux to the front surface at the start of heating) is 2.27×10^7 W/m^2, which is of the order of the heating rate in a rocket nozzle.

As before (Reference 1), it should be noted that the properties and the dimensions used to describe the composite are intended to be illustrative of the general nature of such materials and not necessarily specific to any

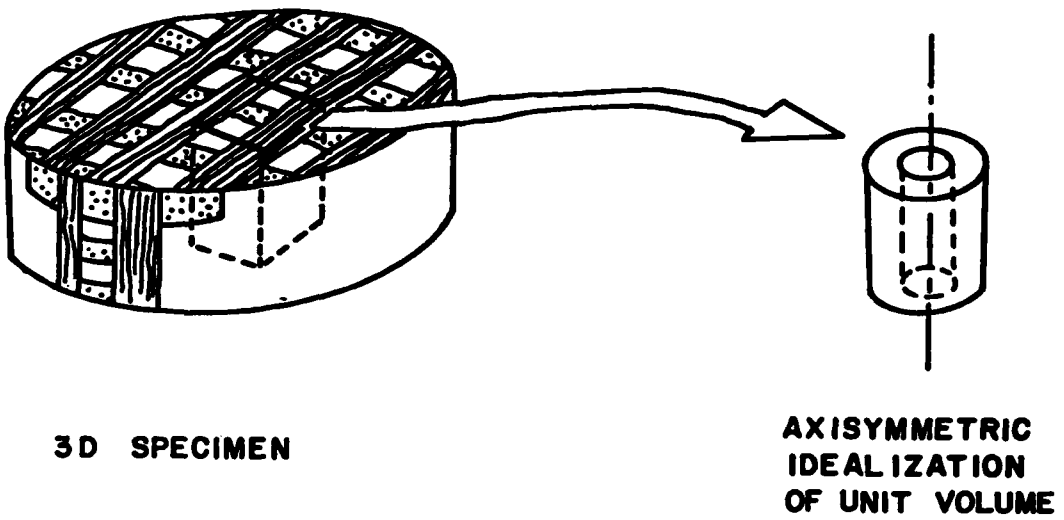

Figure 1. Relation of Volume Analyzed to 3D Composite

Table 1. Material Properties Assumed Analysis

	Material I (Axial Yarn)	Material II (Surrounding Material)
Specific Gravity	1.9	1.9
Specific Heat, cal/gm°C	0.4	0.4
Axial Conductivity, W/cm°C	2.35	0.3
Radial Conductivity, W/cm°C	0.22	0.3
Circumferential Conductivity W/cm°C	0.22	0.3

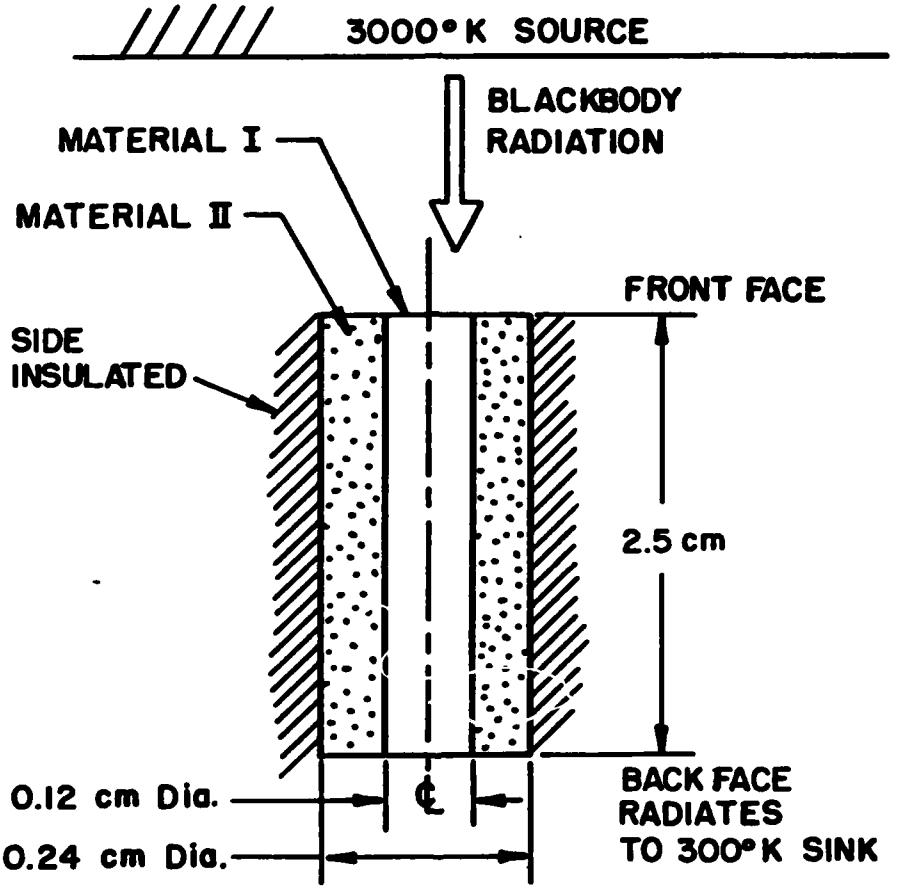

Figure 2. Continuous Heating Case

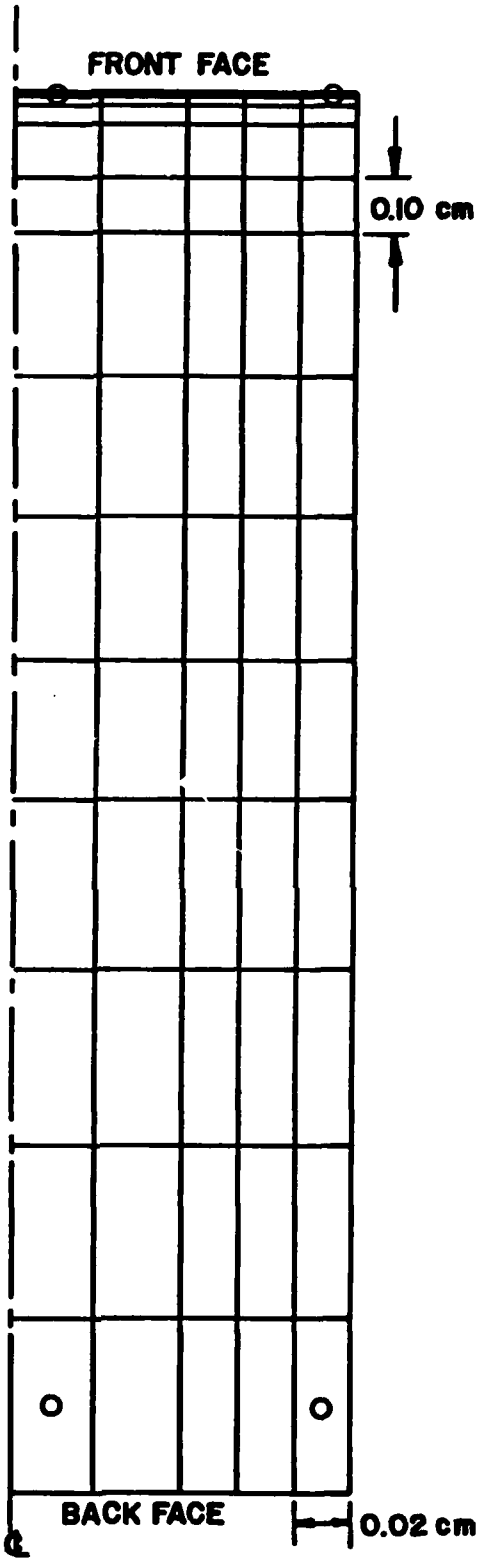

Figure 3. Mesh Used in TASC Calculations. Circles show Nodal Points for which Date is Plotted in Figure 4.

particular carbon-carbon composite. In keeping with the illustrative purpose, and to avoid unnecessary effort in this context, the materials properties were taken to be independent of temperature.

RESULTS

The results are summarized in Table 2 and Figures 4, 5, 6, and 7.

Figure 4 shows the temperature histories of four points in the model, corresponding to the centers of elements marked with small circles in Figure 3. In other words, these points represent

a) the front face near the centerline of a yarn bundle

b) the front face near the outermost region of the surrounding material

c) the back face near the yarn bundle centerline

d) the back face near the outermost region of the surrounding material

We see that a significant temperature gradient exists between constituents at the front face, throughout the period analyzed, whereas the gradient at the backface appears negligible (on the scale of the plot).

The remaining illustrations are intended to show how deep a region near the front face is significantly affected by interconstituent temperature gradients.

Figure 5 shows the calculated temperature gradients along the specimen length, near the yarn bundle centerline and near the outer edge of the surrounding material, at various times during heating. It appears that the depth to which a "significant" gradient exists is about 0.15 cm at all times plotted. Figures 6 and 7 are provided to show the interconstituent temperature differences directly.

Table 2. Selected Results of Computer Calculation

Depth cm	Location in Model		Time, sec					
	Centerline Node	Outer Node	0.21	0.51	1.01	2.01	4.01	7.0
.0025	✓	—	785.1	1028.7	1254.7	1509.7	1778.1	1999.2
	—	✓	1062.3	1291.7	1494.0	1717.8	1950.8	2141.3
.100	✓	—	683.5	932.1	1166.6	1433.0	1714.5	1946.7
	—	✓	699.9	965.1	1203.5	1469.0	1746.5	1973.7
.375	✓	—	404.6	594.5	826.3	1117.6	1442.0	1718.7
	—	✓	378.9	572.1	811.5	1109.2	1437.8	1716.2
.875	✓	—	305.8	348.0	463.2	689.9	1016.3	1342.4
	—	✓	303.4	340.3	453.1	681.5	1010.8	1338.6
1.720	✓	—	300	300.9	311.6	376.4	583.6	915.1
	—	✓	300	300.7	310.1	372.9	579.0	910.7
2.350	✓	—	300	300	301.4	323.8	470.6	789.3
	—	✓	300	300	301.1	322.2	466.7	784.7

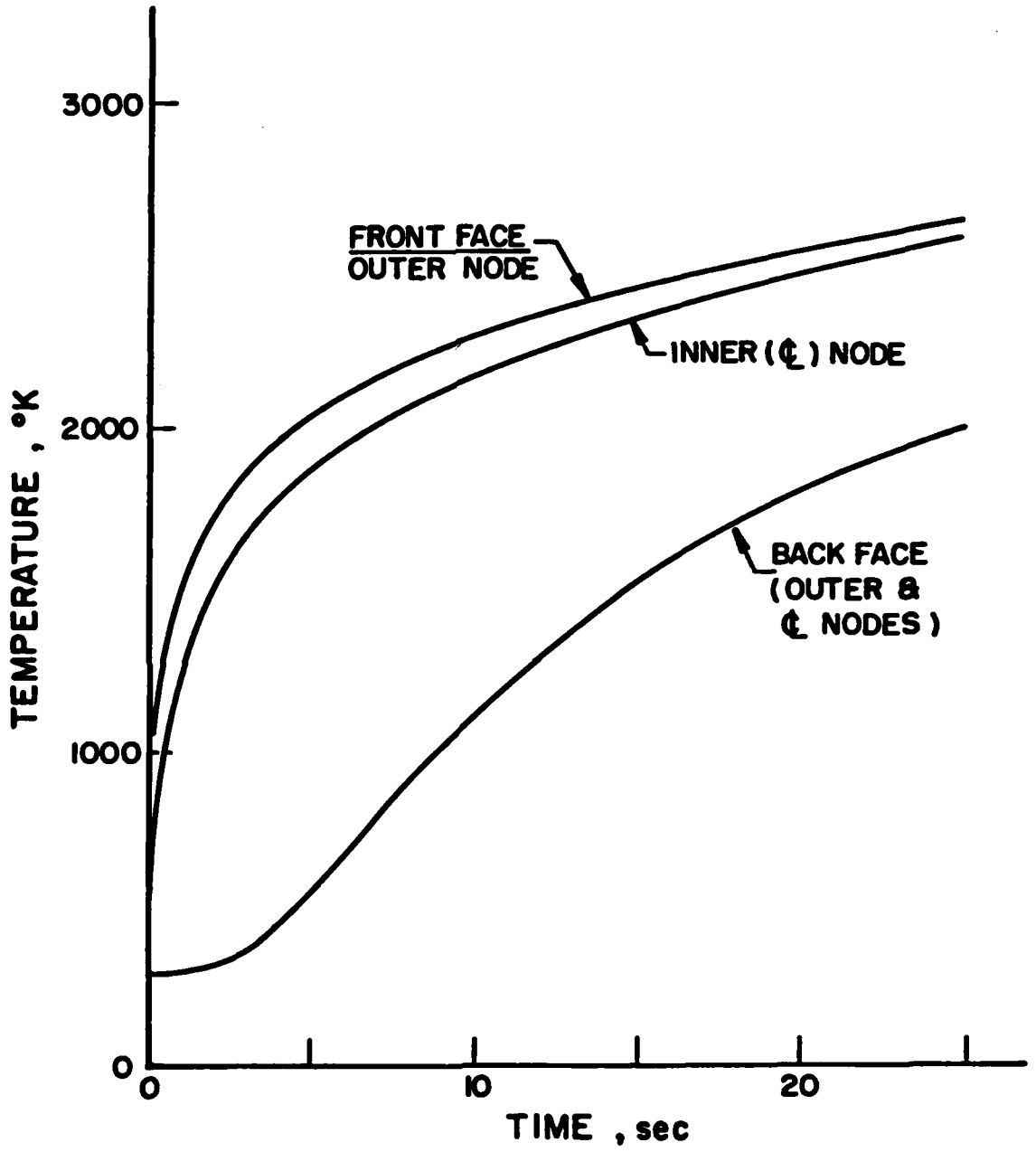

Figure 4. Temperature History of Yarn Bundle Center (Inner Node) and Surrounding Material (Outer Node)

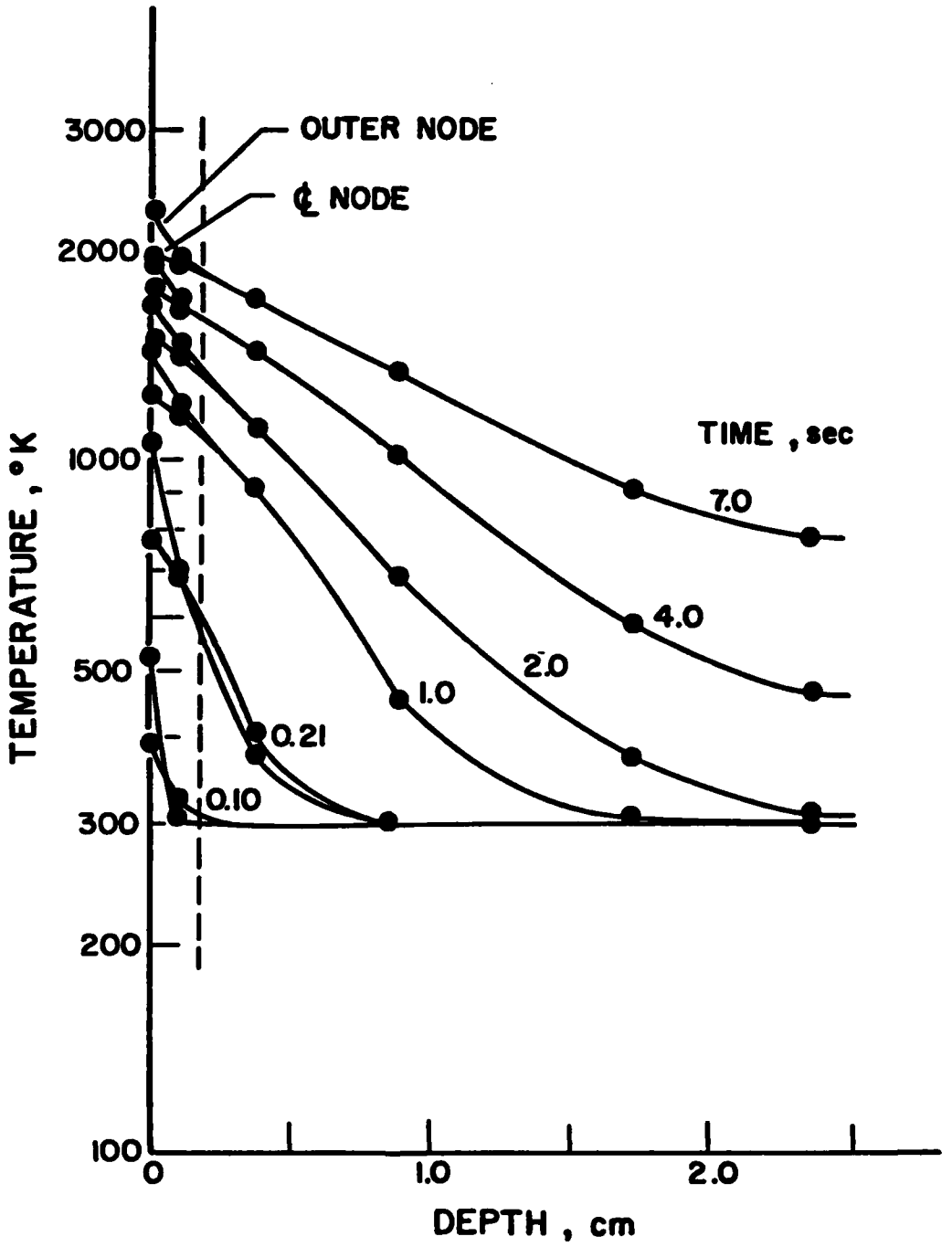

Figure 5. Temperature as a Function of Depth (Distance from Front Face) at Various Times.

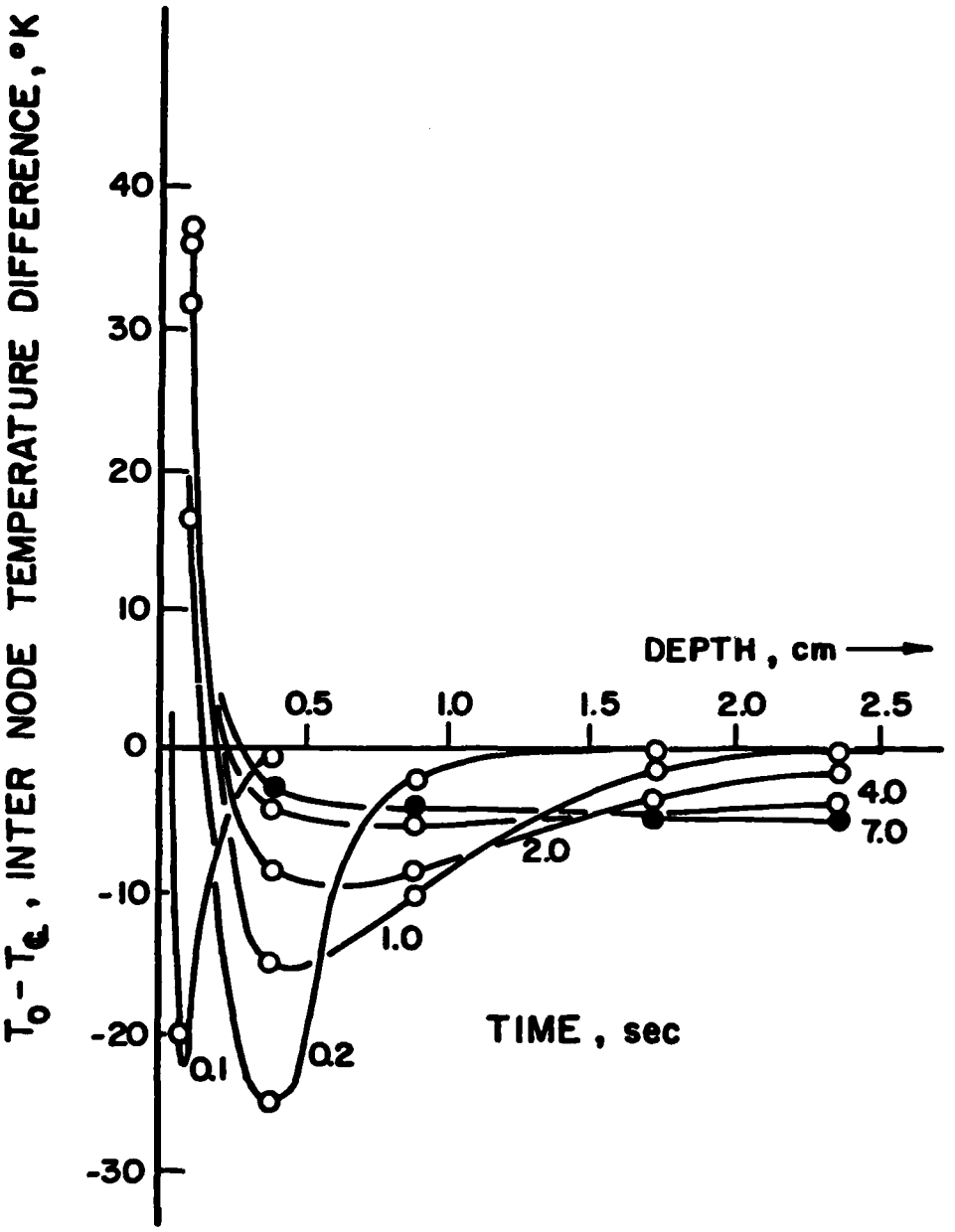

Figure 6. Temperature Difference Between Outer and Inner Nodes as a Function of Depth at Various Times.

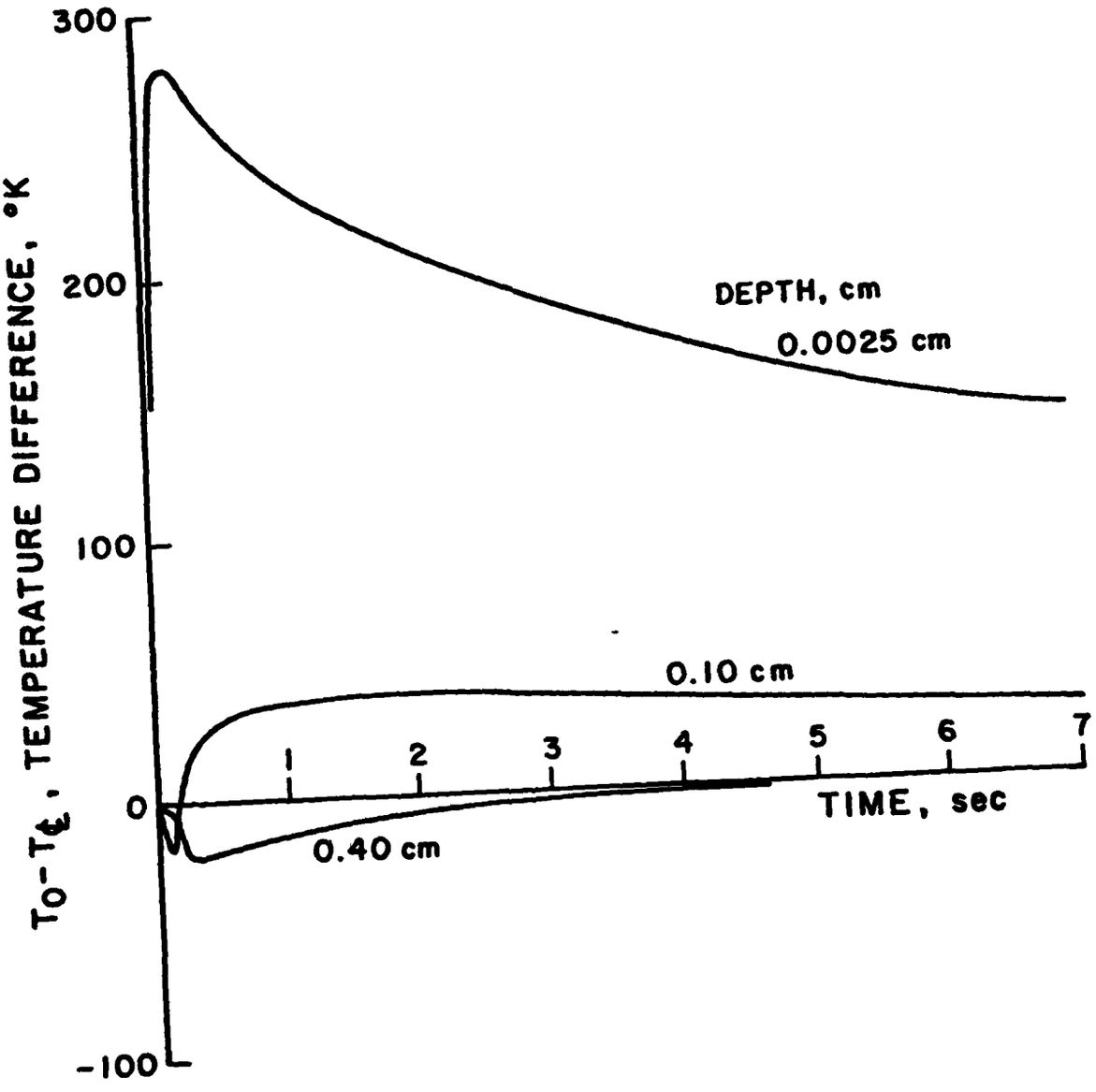

Figure 7. Temperature Difference Between Outer and Inner Nodes as a Function of Time at Various Depths.

Figures 6 and 7 show that, close to the front surface, the less conductive constituent (the surrounding material) is hotter than the more conductive constituent (the yarn bundle), whereas the situation is reversed beyond a depth of about 0.3 cm. Also, the magnitude of the interconstituent gradient is well over 100°C at the surface, but drops to less than 40°C more than about 0.2 cm into the body. At depths greater than about 1 cm, the gradient is always less than about 10°C.

It appears that interconstituent gradients would be of greatest concern within a distance of the heated surface of about a unit-cell dimension (about 0.24 cm, the diameter of the model analyzed, in the present case). As temperature changes of the order of 100°C can be expected to have measurable effects on ablation, we conclude that differences in the conductivity of the constituents are important to consider in the analysis of ablation rates. In this regard, it should be pointed out that the analysis does not directly address ablation, and that it does not consider the effects of possible differences in other relevant properties of the constituents, such as emissivity, kinetics constants, internal surface area, etc.

CONCLUDING REMARKS

The illustrative analysis shows that there is a surface layer within which interconstituent temperaure gradients are significant and beyond which they are negligible. The particular case analyzed supports the intuitive notion (analogous to St. Venant's principle in stress analysis) that the dimension of the surface layer is of the order of the dimension of the hetergeneity. That is, the affected surface layer in this case is approximately as thick as the center-to-center distance between yarn bundles. However, it appears dangerous to generalize to this extent on the basis of one case; surely the ratio of constituent dimensions, the ratio of constituent axial conductivities, the ratios of transverse to axial conductivities, among other factors, will influence the relative thickness of the surface layer. Nevertheless, the results support the view that the material may be treated as homogeneous for the purposes of heat conduction through parts of thickness much greater than

the heterogeneity dimension, but that consideration of heterogeneity is necessary for analysis of events within a layer close to any surface at which heat is transfered at high rates.

References

1. Julius Jortner, Analysis of Transient Temperature Responses in a Carbon-Carbon Composite During Flash-Method Thermal Diffusivity Tests, in Special Edition (Carbon-Carbon Composite Materials) of Current Awareness Bulletin, Issue No. 12, published by Metals and Ceramics Information Center, Battelle Columbus Labs, August 31, 1981. (Also published as an Appendix in Reference 2).

2. R. E. Taylor and H. Groot, Thermophysical Properties of a Carbon-Carbon Composite, Special Report for AFOSR Grant 77-3280, Purdue University Report TPRL 244, May 1981.